HHS Public Access

Author manuscript

Neurobiol Dis. Author manuscript; available in PMC 2024 October 08.

Published in final edited form as:

Neurobiol Dis. 2023 June 01; 181: 106125. doi:10.1016/j.nbd.2023.106125.

Amyloid beta peptides (Aβ) from Alzheimer's disease neuronal secretome induce endothelial activation in a human cerebral microvessel model

Yu Jung Shin[a,b,1], **Kira M. Evitts**[a,b,1], **Solhee Jin**[a], **Caitlin Howard**[a,b], **Margaret Sharp-Milgrom**[c], **Tiara Schwarze-Taufiq**[b,c], **Chizuru Kinoshita**[b,c], **Jessica E. Young**[b,c,*,2], **Ying Zheng**[a,b,*,2]

[a]Department of Bioengineering, University of Washington, Seattle, WA 98109, United States of America

[b]Institute for Stem Cell and Regenerative Medicine, University of Washington, Seattle, WA 98109, United States of America

[c]Department of Laboratory Medicine and Pathology, University of Washington, Seattle, WA 98109, United States of America

Abstract

In Alzheimer's disease (AD), secretion and deposition of amyloid beta peptides (Aβ) have been associated with blood-brain barrier dysfunction. However, the role of Aβ in endothelial cell (EC) dysfunction remains elusive. Here we investigated AD mediated EC activation by studying the effect of Aβ secreted from human induced pluripotent stem cell-derived cortical neurons (hiPSC-CN) harboring a familial AD mutation ($Swe^{+/+}$) on human brain microvascular endothelial cells (HBMECs) in 2D and 3D perfusable microvessels. We demonstrated that increased Aβ levels in $Swe^{+/+}$ conditioned media (CM) led to stress fiber formation and upregulation of genes

*Corresponding authors at: 815 Mercer St., Brotman Building, Room 421, United States of America. jeyoung@uw.edu (J.E. Young), yingzy@uw.edu (Y. Zheng).

[1]These authors contributed equally.

[2]Corresponding authors contributed equally.

Supplementary data to this article can be found online at https://doi.org/10.1016/j.nbd.2023.106125.

Ethics statements

This material is the authors' own original work, which has not been previously published elsewhere. The paper is not currently being considered for publication elsewhere but has been posted as a preprint to bioRxiv. The paper reflects the authors' own research and analysis in a truthful and complete manner.

CRediT authorship contribution statement

Yu Jung Shin: Conceptualization, Data curation, Formal analysis, Funding acquisition, Investigation, Methodology, Visualization, Writing – original draft, Writing – review & editing. **Kira M. Evitts:** Conceptualization, Data curation, Formal analysis, Funding acquisition, Investigation, Methodology, Visualization, Writing – original draft, Writing – review & editing. **Solhee Jin:** Investigation, Writing – review & editing. **Caitlin Howard:** Investigation, Methodology, Writing – review & editing. **Margaret Sharp-Milgrom:** Investigation, Writing – review & editing. **Tiara Schwarze-Taufiq:** Investigation, Formal analysis. **Chizuru Kinoshita:** Investigation. **Jessica E. Young:** Conceptualization, Data curation, Formal analysis, Funding acquisition, Investigation, Methodology, Visualization, Writing – original draft, Writing – review & editing. **Ying Zheng:** Conceptualization, Data curation, Formal analysis, Funding acquisition, Investigation, Methodology, Visualization, Writing – original draft, Writing – review & editing.

Conflict of interest

The authors declare that they have no competing interest. All data needed to evaluate the conclusions in this paper are present in the main paper and/or the Supplementary Materials.

associated with endothelial inflammation and immune-adhesion. Perfusion of Aβ-rich Swe$^{+/+}$ CM induced acute formation of von Willebrand factor (VWF) fibers in the vessel lumen, which was attenuated by reducing Aβ levels in CM. Our findings suggest that Aβ peptides can trigger rapid inflammatory and thrombogenic responses within cerebral microvessels, which may exacerbate AD pathology.

Keywords

Alzheimer's disease; Amyloid beta peptide (Aβ); Endothelial activation; Vascular dysfunction; Disease modeling; 3D microvessels

1. Introduction

Alzheimer's disease (AD) is a progressive neurodegenerative disease and the most common form of dementia (2021 Alzheimer's disease facts and figures, 2021; Brookmeyer et al., 2007). Based on patient's genetic predisposition and the age of onset, AD has been categorized into different types: Sporadic AD accounts for the vast majority of AD cases with patients often exhibiting symptoms later in life; By comparison, familial AD (FAD) accounts for <5% of AD cases but is associated with stronger symptoms and earlier onset. (Behl et al., 2022; Guerreiro and Bras, 2015) The neuropathological hallmarks of AD include the deposition of extracellular amyloid beta (Aβ) plaques, primarily of the Aβ 1–42 isoform (DeTure and Dickson, 2019), formation of intracellular neurofibrillary tangles (NFTs) (Kuchibhotla et al., 2014), and progressive loss of neurons and synapses(Spires-Jones and Hyman, 2014).

Although decades of research have been devoted to understanding the mechanisms of AD development and potential treatments, only a few FDA-approved agents for the treatment of AD are available and no long-term disease-modifying treatments are available (Grammas, 2011). Existing AD research has primarily focused on dysfunctions of cell types in the central nervous system (CNS) such as neurons, astrocytes, and microglia, but growing evidence suggests a role for vascular dysfunction in the development and progression of AD (Grammas, 2011). >90% of patients with Alzheimer's disease (AD) have been found with amyloid deposits along their cerebral vasculature, a condition known as cerebral amyloid angiopathy (CAA) (Blanchard et al., 2020; Ringman et al., 2014; Vidoni et al., 2016; Weller et al., 2009). Such amyloid deposits are known to derive from the pathogenic cleavage of amyloid precursor protein (APP) into insoluble Aβ fragments that oligomerize into amyloid fibrils and plaques (Behl et al., 2020). Aberrant vascular morphology (increased tortuosity of vessels, increased presence of string vessels, thinning of vessel walls, *etc.*), degeneration of vessels in affected brain regions, and decreased cerebral blood flow (CBF) are also apparent in AD (Govindpani et al., 2019). However, the driving factors for vascular malformations present in AD pathogenesis remain unclear.

In vivo, brain microvessels form a vast and complex hierarchical network to regulate transport of nutrients and prevent toxic pathogens and metabolites from entering the CNS. As the interface between circulation and brain tissue, endothelial cells (ECs) play a critical role in building a strong blood-brain barrier (BBB). In their healthy state, brain ECs

express tight junction proteins to limit the diffusion of molecules into the brain (Tietz and Engelhardt, 2015); when activated in response to pro-inflammatory signals, brain ECs exhibit (1) loss of vascular integrity, (2) increased expression of adhesion molecules, such as intercellular adhesion molecule 1 (ICAM-1) and vascular cell adhesion molecule 1 (VCAM-1), (3) upregulation of human leukocyte antigen molecules, (4) exocytosis of Weibel-Palade bodies (WPB) containing P-selectins and von Willebrand Factor (VWF), indicating a prothrombotic state following endothelial injury, (5) increased secretion of cytokines (IL-8, IL-12), and (6) assembly of stress fibers (Gupta et al., 2005; Lip and Blann, 1997a; Peng et al., 2019).

In patients with AD, serum and plasma analysis showed increases in plasma concentration of VWF and soluble endothelial adhesion proteins including *E*-selectin, P-selectin, ICAM-1 and VCAM-1 (Borroni et al., 2002; Govindpani et al., 2019; Järemo et al., 2013; Kelleher and Soiza, 2013; Wolters et al., 2016; Zuliani et al., 2008), suggesting EC activation and systemic inflammation. Activation of the endothelium would convert the normally unreactive endothelial surface into an adhesive surface capable of binding platelets and leukocytes, and possibly also erythrocytes. These vascular activation events could initiate the coagulation cascade, leading to microvascular occlusion in brain microvessels (Yau et al., 2015). In addition, enhanced expression of other adhesion molecules such as ICAM-1 and VCAM-1 would assist the rolling and firm adhesion of leukocytes to EC surface, promoting extravasation of immune cells into the brain parenchyma (Cook-Mills et al., 2010; Zenaro et al., 2017). Neutrophil recruitment to the CNS *via* adhesion molecules is also known to promote activation of microglia and astrocytes inducing neuronal damage (Zenaro et al., 2015).

Despite the debilitating nature of vasculopathies in AD, studies of human AD-mediated vascular dysfunction are limited as it is challenging to study cellular function non-invasively in the human brain. *In vitro* cultures of EC monolayers have shown that exogenously applied Aβ peptides led to nuclear and mitochondrial DNA damage, cell death, increased BBB permeability and increased monocyte adhesion on ECs (Grammas, 2011; Gupta et al., 2005; Suhara et al., 2003; Xu et al., 2001). In bovine aortic EC cultures, Aβ 1–42 was found to induce endothelial dysfunction by raising intracellular calcium levels *via* calcium-permeable Aβ channels (Bhatia et al., 2000). These 2D *in vitro* studies, however, lack proper vascular architecture, lack *in vivo* flow characteristics, and apply exogenous Aβ at micromolar doses, which is higher than the average concentration, at picomolar levels, of Aβ measured in the human brain (Kass et al., 2022). It remains elusive to what extent Aβ peptides drive human brain microvascular injuries and dysfunctions in AD conditions.

Transgenic mouse models of AD are often utilized to show cerebrovascular phenotypes, however, not all the models show the same aberrations and they do not always occur at the same time (Szu and Obenaus, 2021). For example, decreased vessel density, a common vascular alteration in human AD, is observed in only one of the ten most common AD mouse models, and depending on the mouse line, the onset of vascular amyloid deposition can occur anywhere between 3 months and 24 months of age (Szu and Obenaus, 2021). Furthermore, these animal models often have non-physiologic expression of a number of AD-related transgenes. Hence there is a critical need to evaluate the role of Aβ in

AD-associated vascular dysfunction in a system that structurally and functionally mimics human brain vasculature and includes accurate Aβ levels.

More recently, advances in microfluidic-based techniques enabled modeling of the 3D BBB with perfusable lumens that can recapitulate the biochemical and biophysical perturbations occurring in cerebral blood vessels (Shin et al., 2019; Zheng et al., 2015). Culturing ECs under flow improves EC homogeneity, homeostatic control, EC alignment with flow, vascular development, and EC proliferation (Choublier et al., 2022; Helle et al., 2020; Redd et al., 2019). In primary HBMECs, flow has also been shown to increase the tightness of junctions in vascular models, which significantly decreased EC permeability, better reflecting the highly impermeable barrier of the *in vivo* BBB (Cucullo et al., 2007). Hence, 3D perfusable human cerebral vascular models provide timely opportunities for studying the responses of human brain ECs and microvessels to the increased levels of secreted Aβ in AD in physiological and pathological-relevant conditions.

In this study, we utilized primary HBMECs and established a 3D perfusable human brain microvessel platform to study AD-associated endothelial activation. We modeled the AD response by perfusing these microvessels with neuronal secretomes, collected as conditioned medium (CM) from human neuronal cultures. These neurons were differentiated from human induced pluripotent stem cells (hiPSCs), that harbor the APP Swedish mutation KM670/671NL (APPSwe). This mutation increases Aβ secretion by enhancing amyloidogenic APP cleavage by β-secretase 1 (BACE1) and is causative for early-onset FAD (Haass et al., 1995; Young et al., 2018). Cells with AD mutations, including the Swedish mutation, have been used to study blood-brain barrier (BBB) changes in AD and CAA (Park et al., 2018; Penney et al., 2020a). One recent study demonstrated that conditioned media (CM) collected from hiPSC-derived APPSwe neurons led to increased permeability in 2D monolayers of proliferating brain ECs, while WT CM did not affect permeability (Williams et al., 2022), suggesting that this CM study can recapitulate features of BBB dysfunction seen in AD brain.

We compared the endothelial alterations induced by treatment with CM from cortical neuron cultures differentiated from APPSwe hiPSCs (hiPSC-CNs) and their isogenic wild-type (WT) control cell lines. In 2D, treatment of HBMECs with CM from AD hiPSC-CNs led to cytoskeletal reorganization and upregulation of genes involved in immune cell interaction with ECs. In 3D flow-directed brain microvessels, perfusion of CM from APPSwe hiPSC-CNs elicited acute endothelial activation and formation of transluminal VWF fibers, suggesting the initiation of thrombotic microangiopathy within the luminal space. By showing reduced endothelial activation to CM from neurons deficient in APP expression (APP^{KO}), or from APPSwe cells treated with a β-secretase inhibitor (BACEi), we demonstrated the pivotal role of Aβ in EC activation. Our findings highlight that increased Aβ levels secreted by AD neurons lead to endothelial activation in brain microvessels. This suggests that Aβ has a direct role in eliciting acute hemostasis and vascular inflammation in the cerebrovasculature of AD patients.

2. Results

2.1. APPSwe hiPSCs-CNs secretes Aβ in a genotype-dependent manner

To investigate the effect of AD neuron derived paracrine signaling on HBMECs, we differentiated hiPSCs from an established cell line harboring the APPSwe mutation into cortical neurons (CNs) (Penney et al., 2020b; Young et al., 2018) (Fig. 1A,B). Following a previously published protocol (Knupp et al., 2020; Rose et al., 2018), neural progenitor cells (NPCs) were first differentiated from hiPSCs for 3 weeks, followed by another 3 weeks of differentiation into neurons. At the end of the 3-week differentiation, CNs were enriched in the cultures, as marked by robust immunofluorescent staining for the neuron marker MAP2 (Fig. 1B). hiPSC lines homozygous ($Swe^{+/+}$) and heterozygous ($Swe^{+/WT}$) for the APPSwe mutation were used to generate hiPSC-CNs (Fig. 1A). Control hiPSC-CNs were made using the parental wild type ($Swe^{WT/WT}$) line for the APPSwe lines, and an APP knock out (APP^{KO}) cell line was used as an additional control (Young et al., 2018, 2015).

After 3-weeks of differentiation, CM was collected from hiPSC-CN cultures and measured for their Aβ 1–42 and 1–40 levels using an ELISA assay (Fig. 1C). CM collected from $Swe^{+/+}$ and $Swe^{+/WT}$ hiPSC-CNs showed increased Aβ 1–42 and 1–40 levels compared to controls, with the highest mean in the $Swe^{+/+}$ line for Aβ 1–42 (487 pg/mL) and 1–40 levels (5431 pg/mL). The $Swe^{+/WT}$ line showed significantly lower Aβ 1–42 (137 pg/mL) and Aβ 1–40 (1033 pg/mL) levels compared to $Swe^{+/+}$, but significantly higher than that collected from the $Swe^{WT/WT}$ (Aβ 1–42 at 50 pg/mL and 1–40 at 385 pg/mL). These results confirm that the APPSwe neurons secrete increased levels of Aβ and may be a viable way to mimic paracrine signals from neurons in the AD brain.

2.2. Paracrine signaling from neurons induces endothelial activation and cytoskeletal reorganization in 2D monolayer culture

Under stress, endothelial cells may be activated, which leads to the formation of stress fibers (Peng et al., 2019). We next treated HBMECs in a 2D monolayer (Fig. 2A (i)) with CM obtained from hiPSC-CN cultures to evaluate the paracrine effect of neurons on HBMECs. Four media groups were tested to assess endothelial activation after a 6-h treatment: $Swe^{+/+}$ CM, $Swe^{+/WT}$ CM, $Swe^{WT/WT}$ CM, and unconditioned media (UCM). Upon treatment with $Swe^{WT/WT}$ CM, HBMECs exhibited quiescent cytoskeletal structures characterized by a cortical actin rim around the peripheral junctions (Fig. 2A i and ii-arrows). In comparison, $Swe^{+/+}$ CM and $Swe^{+/WT}$ CM treated HBMECs showed reorientation of actin fibers into elongated stress fibers with increased cell polarity (Fig. 2A iii and iv-arrowheads), suggesting their activated state. In particular, $Swe^{+/+}$ CM treated HBMECs show significant retraction of endothelial cells (Fig. 2A (iv-arrowheads)), characterized by degradation of vascular endothelial cadherin (VECAD) junctions in areas of retraction (Fig. 2A (viii-asterisk)), and increased gap formation between adjacent ECs.

2.3. RNA sequencing (RNAseq) reveals endothelial activation signatures in CM treated HBMECs

To understand the transcriptomic changes in endothelial cells following CM treatment, we sequenced RNA collected from 2D HBMECs that were treated with two batches of

$Swe^{+/+}$ CM, $Swe^{WT/WT}$ CM, and UCM. Principal component analysis (PCA) showed that individual UCM, $Swe^{WT/WT}$, and $Swe^{+/+}$ CM treated groups clustered together (Fig. 2B). In particular, the UCM cluster is distinctly separated from the $Swe^{WT/WT}$ and $Swe^{+/+}$ clusters, suggesting that neuronal secretomes had a large effect on EC function compared to UCM. Clusters also form within the same media batch groups, with distinct cluster presentations for $Swe^{WT/WT}$ and $Swe^{+/+}$ groups. Batch-to-batch variation appeared to exist in the CM obtained, leading to overlaps among clusters, which is likely due to the inherent heterogeneity of hiPSC-CNs and secretome production (Supplemental Fig. 1). For analysis of RNAseq, we combined both batches for unbiased representation of transcriptomes that were differentially expressed between $Swe^{WT/WT}$ and $Swe^{+/+}$ treated ECs. Results showed 10 genes that were differentially expressed between HBMECs treated with $Swe^{WT/WT}$ CM and $Swe^{+/+}$ CM (Fig. 2C). This includes upregulation of genes associated with endothelial adhesion molecules: SELE (~7-fold change), VCAM-1 (~6-fold change) and ICAM-1 (~3-fold change) (Fig. 2D and E). CCL2 and SDCBP2 were also upregulated, which supports the presence of higher levels of inflammatory cytokines in $Swe^{+/+}$ CM. Down-regulated genes include: INPP5J, TSPYL5, SOCS3 and PDZD7 (Fig. 2C and D). Downregulation of the TSPYL5 gene, known to be associated with endothelial proliferation and tube formation, suggests angiogenic ability may be attenuated in ECs with AD exposure (Na et al., 2019). GO term and KEGG pathway analysis showed upregulation of pathways related to leukocyte adhesion, cellular extravasation, and endothelial inflammation (Fig. 2F). 24-h treatment of HBMECs with $Swe^{+/+}$ CM and $Swe^{WT/WT}$ CM confirmed increased VCAM-1 expression on the endothelial surface upon stimulation with $Swe^{+/+}$ CM (Supplemental fig. 2).

Overall, both phenotypic and transcriptomic analyses of HBMECs suggest that ECs are activated by neuronal secretomes in AD CM through cytoskeletal reorganization, and transcriptional alteration. These data indicate that paracrine signaling from AD neurons elicits a pro-inflammatory, pro-thrombotic, and anti-angiogenic environment in brain ECs.

2.4. $Swe^{+/+}$ conditioned media induces endothelial activation in 3D flow-mediated engineered cerebral microvessels

The endothelium *in vivo* forms an intact lumen and 3D network structure, responding to flow and cytokines synchronically. When activated, the endothelium is known to release granules, such as VWF, which can extend and multimerize into large fibers, under flow, to bind platelets and other blood cells (Zheng et al., 2015). Such activation denotes a shift of the endothelium toward a prothrombotic phenotype and has been shown as a signature phenomenon in 3D microvessels (Zheng et al., 2015). We examined whether $Swe^{+/+}$ CM would induce rapid activation of 3D flow-mediated engineered cerebral microvessels. Using the engineered microvessel method previously developed by our lab (Zheng et al., 2012), we created devices with a double grid geometry (8 × 8) for microvessels with a feature height of 150 μm (Fig. 3A) and seeded with HBMECs at a concentration of 7×10^6 cells/mL. After culture for 5–7 days under gravity-driven flow, a continuous and confluent endothelium was established in 3D engineered cerebral microvessels (Fig. 3A).

We then perfused cerebral microvessels with different CM for 1 h under gravity-driven flow (Fig. 3A) and evaluated the formation of VWF fibers in the vessel lumen. Treatment of

vessels with $Swe^{+/+}$ media led to the formation of large transluminal VWF fibers throughout the vessels (Fig. 3B (green) and 3C), which was not observed upon perfusion with CM from the $Swe^{WT/WT}$ line or UCM. The extended VWF fibers in the vessel lumen expose binding sites for platelets, which could initiate thrombosis in vessels (Drakeford and O'Donnell, 2017). We next perfused washed platelets isolated from whole blood, stained for the platelet marker CD41a, through the microvessels. Upon perfusion, platelets readily bound to VWF fibers in the $Swe^{+/+}$ condition, but there was minimal binding in vessels with no VWF fibers (UCM and $Swe^{WT/WT}$) (Fig. 3B (red)). Using VWF staining and platelet perfusion, two types of VWF fibers were identified in perfused microvessels, including transluminal fibers, seen as large fibers in the center of the vessel lumen, and wall fibers, as small fibers found on the wall of the vessels that are marked by platelet strings (Supplemental Fig. 3). Brightfield and scanning electron microscopy of the $Swe^{+/+}$ CM treated microvessels showed that large aggregates of platelets are bound to ultra-large transluminal VWF fibers (Fig. 3C(i)) whereas single platelet binding occurred on wall string fibers. (Fig. 3C(ii) and 3D). Quantification of wall and transluminal fibers in vessels perfused with $Swe^{+/+}$ CM showed a significant increase in transluminal and total fibers, and a trend toward increased wall fiber formation across several replicates compared to controls (UCM and $Swe^{WT/WT}$) (Fig. 3E).

Furthermore, we observed that in brain microvessels perfused with $Swe^{+/+}$ CM, leukocytes were able to bind to the endothelial surface and initiate a tethering and rolling response. This suggests that endothelial cells were activated by CM with higher Aβ concentrations which facilitated immunoadhesion within the microvessels (Supplemental Fig. 4; Supplemental Video 1). These results suggest that perfusion of engineered microvessels with CM with high Aβ levels can induce EC activation and VWF fiber formation that is not present in vessels perfused with CM from cell lines with low Aβ production.

2.5. Knocking out APP and inhibiting the beta-secretase enzyme BACE1 with a small molecule inhibitor (BACEi) attenuate endothelial cell activation and VWF release

To test whether the increased level of Aβ in our APPSwe CM is a driving factor for endothelial activation, we perfused microvessels with CM from $Swe^{+/+}$, $Swe^{+/WT}$, and $Swe^{WT/WT}$ hiPSC-CNs treated with a BACE1 inhibitor (BACEi). BACEi inhibits BACE1 function and prevents the amyloidogenic cleavage of APP into Aβ (Fig. 4A) (Chow et al., 2010; Satir et al., 2020). CM was collected from cultures of hiPSC-CNs after treatment with either BACEi (25 nM) or vehicle control (DMSO) for 72 h (Fig. 4B). ELISA measurements showed a statistically significant 44% decrease in Aβ 1–42 levels (DMSO: 170 pg/mL, BACEi: 75.4 pg/mL) and 45% decrease in Aβ 1–40 levels (DMSO: 1504 pg/mL, BACEi: 683 pg/mL) in $Swe^{+/+}$ BACEi treated cultures compared to DMSO controls (Fig. 4C and Supplemental Fig. 5). In $Swe^{+/WT}$ cultures, BACEi treatment led to a statistically significant 38% decrease in both Aβ 1–42 (DMSO: 101 pg/mL, BACEi: 38.1 pg/mL) and 1–40 (DMSO: 794 pg/mL, BACEi: 298 pg/mL) levels compared to controls. In $Swe^{WT/WT}$ cultures, BACEi treatment led to a 28% reduction in Aβ 1–42 levels (DMSO: 32.4 pg/mL, BACEi: 9.14 pg/mL) and 26% reduction in Aβ 1–40 levels (DMSO: 264 pg/mL, BACEi: 69.1 pg/mL).

Furthermore, perfusion of cerebral microvessels with $Swe^{+/+}$ and $Swe^{+/WT}$ BACEi CM led to the formation of only a few VWF fibers, in contrast to the significantly larger number of fibers in $Swe^{+/+}$ and $Swe^{+/WT}$ DMSO CM conditions (Fig. 4D). Quantification of the fiber number in each media condition confirms this consistent and significant decrease across multiple replicates in BACEi treated conditions compared to the corresponding DMSO controls (Fig. 4F). In our $Swe^{WT/WT}$ control line, there was little to no fiber formation in both the BACEi and DMSO conditions as expected (Fig. 4D).

To test whether VWF fibers would form in the presence of neuronal secretomes but in the complete absence of Aβ or other components of amyloidogenic APP processing, CM was collected from APP^{KO} hiPSC-CNs (Young et al., 2018). Analysis of Aβ 1–42 and 1–40 levels showed that CM from the APP^{KO} line did not secrete detectable levels of Aβ peptides as expected (Fig. 4C and Supplemental Fig. 4). When APP^{KO} CM was perfused through brain microvessels, no transluminal VWF fibers were observed in the vessel lumen (Fig. 4E and F).

Notably, the number of VWF fibers in the HBMEC microvessels appears to have a positive linear correlation with the levels of Aβ 1–42, across all the media groups (Fig. 4G). For example, $Swe^{+/+}$ DMSO CM had Aβ 1–42 levels of 170 pg/mL and led to maximal fiber production of, on average, 45 VWF fibers per vessel. In contrast, $Swe^{+/WT}$ DMSO CM had 41% less Aβ 1–42 (101 pg/mL) and 46% less average VWF fiber production (24 VWF fibers per vessel) compared to $Swe^{+/+}$ DMSO CM, demonstrating a strong correlation between Aβ 1–42 levels and VWF fiber production (Fig. 4G).

Next, we performed immunoprecipitation (IP) of Aβ peptides in $Swe^{+/+}$ and $Swe^{WT/WT}$ CM to investigate whether the presence of Aβ peptides in $Swe^{+/+}$ was necessary for inducing EC activation and VWF fiber formation in engineered brain microvessels. Aβ peptides in $Swe^{WT/WT}$ and $Swe^{+/+}$ CM were precipitated using the anti-Aβ 6E10 antibody. An ELISA assay following IP confirmed successful removal of Aβ peptides from $Swe^{+/+}$ and $Swe^{WT/WT}$ CM. (Supplemental fig. S6). Next, control $Swe^{WT/WT}$ and $Swe^{+/+}$ CM (control CMs) and immunoprecipitated $Swe^{WT/WT}$ and $Swe^{+/+}$ CM (IP CMs) were perfused in engineered brain microvessels. VWF staining in the microvessels revealed a reduced number of fibers formed in $Swe^{+/+}$ IP CM compared to its $Swe^{+/+}$ control CMs. Furthermore, perfusion of both $Swe^{WT/WT}$ control and IP CMs resulted in a lack of VWF fibers, further supporting that Aβ peptides were an important component of the CM for inducing EC activation and VWF fiber formation.

Taken together, the number of fibers formed in BACEi treatment, APP^{KO} CM perfusion and Aβ-depleted CM perfusion relative to Aβ peptide levels suggest that Aβ is an essential component of the CM for inducing EC activation and VWF fiber formation in engineered cerebral microvessels.

2.6. Analysis of pro-inflammatory cytokines and pTau from the neuronal secretome further supports increased Aβ levels as a primary factor in endothelial cell activation

To determine whether secretion of pro-inflammatory cytokines into our CM acts as a confounding factor driving EC activation, independent of Aβ, we performed a multiplexed

cytokine ELISA assay. We screened untreated CM from APP^{KO}, $Swe^{WT/WT}$, $Swe^{+/WT}$, and $Swe^{+/+}$ hiPSC-CNs and CM from DMSO and BACEi treated $Swe^{WT/WT}$, $Swe^{+/WT}$, and $Swe^{+/+}$ hiPSC-CNs. APP^{KO} CNs were not treated with DMSO or BACEi due to the lack of APP production and therefore were not included in those analyses. Our cytokine panel included 9 pro-inflammatory cytokines and chemokines: TNF-α, IP-10, IL-8, IL-6, IL-15, IL-1β, IFN-β, IFN-α2a, and Eotaxin.

We observed that there was no trend toward increased cytokine secretion in untreated $Swe^{+/+}$ and $Swe^{+/WT}$ CM as compared to $Swe^{WT/WT}$, or APP^{KO} for any of the measured cytokines (Supplemental Fig. 6). This suggests that the increased number of VWF fibers observed in microvessels treated with $Swe^{+/+}$ and $Swe^{+/WT}$ CM was not driven by the cytokines present in CM. Surprisingly, for the majority of cytokines, IP-10, IL-8, IL-6, IFN-β, IFN-α2a, and Eotaxin, the highest cytokine levels were observed in our control CM ($Swe^{WT/WT}$ or APP^{KO}). Additionally, across all measured cytokines, we saw no trend suggesting BACEi CM had decreased cytokine levels compared to DMSO CM (Supplemental Fig. 7).

To rule out secreted phosphorylated tau (pTau) as a potential driver of the EC activation, we performed a pTau and total Tau (tTau) ELISA assay to quantify pTau levels in our CM. We screened media from APP^{KO}, $Swe^{WT/WT}$, $Swe^{+/WT}$, and $Swe^{+/+}$ hiPSC-CNs. We found that pTau secretion into the CM was negligible for all of the measured lines and the levels of pTau within CM did not correlate with the EC activation we observed in microvessels treated with $Swe^{+/+}$ and $Swe^{+/WT}$ CM (Supplemental fig. S8).

Overall, we conclude that that the APPSwe mutation does not drive increased pro-inflammatory cytokine secretion from neuronal cultures, treatment of CNs with a BACEi does not lead to reduced cytokine secretion, and pTau secretion in conditioned media is negligible across all lines and does not correlate with EC activation. Taken together, our results suggest that the endothelial activation observed in our studies is strongly correlated to the Aβ levels in neuronal secretomes.

3. Discussion

AD research has traditionally been focused on neuronal and glial dysfunction. Despite evidence of vascular contributions that precede the clinical diagnosis of AD, endothelial alteration in AD has been relatively poorly explored, partly due to the lack of proper humanized models. In this study, we used hiPSC-derived neurons harboring the APPSwe mutation, together with primary HBMECs and engineered 3D brain microvessels to investigate AD-associated vascular dysfunction. We validated that $Swe^{+/+}$ mutation led to a higher concentration of Aβ deposition in CM compared to $Swe^{WT/WT}$ control. The measured Aβ levels were in the picomolar range, which is more physiologically relevant than micromolar concentrations of exogenous Aβ peptides often applied (Bhatia et al., 2000; Suhara et al., 2003; Xu et al., 2001). We demonstrated that these AD-mimicking CM caused transcriptomic and phenotypic upregulation of adhesion molecules in HBMECs. Perfusion of this high Aβ-containing $Swe^{+/+}$ CM in 3D microvessels elicited rapid endothelial activation, following 1-h treatment of brain microvessels, characterized by the formation of

prothrombotic VWF fibers and leukocyte binding on vessel lumen. Inhibiting Aβ production in APPSwe with a BACE1 inhibitor or APP^{KO} attenuated the endothelial activation.

Our findings show a threshold level of neuronally secreted Aβ peptide that leads to endothelial cell activation and acute VWF release and fiber formation. This process could serve as an early source of vascular dysfunction in AD. Measuring plasma Aβ as a biomarker for AD has produced conflicting results in the literature throughout the different stages of AD pathogenesis (Janelidze et al., 2016; Lim et al., 2020; Nakamura et al., 2018; Rissman et al., 2012). Although plasma and CSF levels of Aβ are decreased in some AD patients compared to healthy individuals (Hansson et al., 2019; Mehta et al., 2000), the majority of FAD patients develop CAA, a condition characterized by Aβ deposits along the small vessels in the brain(Vidoni et al., 2016). This suggests an increase in circulating Aβ levels at or prior to the disease onset, which may increase endothelial activation, induce pro-coagulative states, disrupt cerebral blood flow and increase immune cell activation, all of which can further induce deposition of Aβ in cerebral blood vessels. The increased deposition of Aβ, as Aβ fibrils and plaques along the vessel wall, could be a reason for the decreased plasma and CSF Aβ.

Our results suggest that neuronally derived Aβ peptides can drive the EC activation and dysfunction in otherwise healthy vessels. We show that the APPSwe mutation in our hiPSC-CNs led to increased Aβ 1–42 and Aβ 1–40 peptide secretion in a genotype-dependent manner (Fig. 1C). Because the amounts of Aβ we measure from our CM are in the ng/mL concentrations, this suggests that even small amounts of pathogenic Aβ peptides may lead to significant changes in vascular structure and function, which can occur early in disease progression, prior to the formation of higher-order Aβ assemblies. Our observations support increasing evidence that vascular dysfunction may precede the onset of pathophysiological and cognitive symptoms in AD (Govindpani et al., 2019). Our results also support that Aβ peptides may be involved early in AD pathogenesis.

AD-related changes in brain vasculature are associated with responses to inflammatory signals, oxidative stress, adaptive immune responses, and upregulation of endothelial adhesion molecules (Chen et al., 2020; Propson et al., 2021; Schaum et al., 2020; Yang et al., 2022; Yousef et al., 2019). In particular, endothelial VCAM-1 expression (Yousef et al., 2019) and increased binding of lymphocytes to VCAM-1 in the brains of AD patients (Gate et al., 2020) emphasize the role of endothelial adhesion molecules in AD. Using RNAseq, we revealed that endothelial cells respond to paracrine signals from neurons of $Swe^{+/+}$ FAD mutation by enhancing expression of genes associated with inflammatory responses and immunoadhesion. *E*-selectin, ICAM-1 and VCAM-1, precursor genes for adhesion molecules in endothelial cells, were significantly upregulated in HBMECs treated with $Swe^{+/+}$ CM. Increased expression of adhesion molecules can recruit circulating leukocytes in inflamed vessel lumens and assist infiltration of immune cells to the CNS compartment. Facilitating neutrophil recruitment to the CNS *via* adhesion molecules can promote activation of microglia and astrocytes and initiate neuroinflammation and neuronal damage (Lee et al., 2018). CCL2 was also significantly upregulated in $Swe^{+/+}$ CM treated HBMECs which can elicit endothelial retraction and breakdown of the blood-brain barrier, allowing for the accumulation of neurotoxic chemokines and plasma proteins (Chui and Dorovini-Zis,

2010). Our transcriptional analysis highlights the molecular connection between pathogenic Aβ levels, vascular inflammation, and hemodynamic dysfunction. As vascular inflammation manifests in the early stages of AD neuropathology, the inflammation cycle may exacerbate AD pathology and augment cognitive impairment.

We showed, for the first time, that perfusion of Aβ-rich CM through 3D human brain microvessels can promote acute release of VWF from endothelium and formation of ultra-large transluminal fibers in the 3D vessel lumen. We show a strong linear correlation between Aβ levels in the CM and the number of transluminal VWF fibers in 3D microvessels. Perfusion of $Swe^{+/+}$ CM with high Aβ concentrations led to large VWF fiber formation and high level of platelet binding. Attenuated Aβ 1–42 and Aβ 1–40 levels in CM with BACE1 inhibition in APPSwe CNs significantly reduced VWF fiber formation in 3D human brain microvessels. CM from APP^{KO} CNs with no detectable secretion of Aβ 1–42 and Aβ 1–40, correspondingly led to no transluminal VWF fiber formation in vessels. Pro-inflammatory cytokine levels in our APPSwe CM did not increase in a genotype-dependent manner or decrease upon BACEi treatment, suggesting that proinflammatory cytokine secretion is not a key driver of the EC activation we observed. These data demonstrate a strong correlation between concentrations of Aβ, endothelial VWF release, and endothelial activation in human brain microvessel models.

VWF is a multimeric protein that is released from WPB either constitutively from quiescent ECs, or acutely during acute activation of ECs (Lip and Blann, 1997b; Michaux and Cutler, 2004). Upon release from WPB, VWF unfurls its multimeric structures into elongated strings under flow, exposing crosslinking sites to bind platelets and assemble into its ultra-large fiber structure (Fu et al., 2017). Although how Aβ initiates WPB exocytosis is not in the scope of this work, past studies shed light on possible calcium-dependent mechanisms of Aβ induced WPB release. Transient exposure of Aβ 1–40 has been linked with disruption of calcium homeostasis in brain endothelial cells (Fonseca et al., 2015; Kook et al., 2012). Short-term treatment of Aβ in rat brain endothelial cells has been found to increase mitochondrial and cytosolic calcium release (Parodi-Rullán et al., 2019), which could promote exocytotic formation and exocytosis of WPBs (Cleator et al., 2006; Mietkowska et al., 2019). Release of VWF leads to fiber formation within the vessel lumens that attract platelets, bind directly to P-select glycoprotein ligan-1 on polymorphonuclear leukocytes, and recruit leukocytes for subsequent diapedesis and promote inflammatory and thrombotic events (Chen et al., 2004; Petri et al., 2010). By comparing the perfusion outcomes of $Swe^{+/+}$ CM with $Swe^{WT/WT}$, $Swe^{+/WT}$ and that with BACEi treatment and APP^{KO} media, our results demonstrated that Aβ peptides are an important component of the CM leading to EC activation. Future human studies are needed for remaining questions such as whether there is an Aβ concentration threshold below which EC activation will not occur and above which EC dysfunction will be initiated. Understanding the minimum Aβ peptide levels required to cause EC dysfunction could help inform therapeutic strategies for AD. Overall, the results of our study have enhanced our understanding of the role of Aβ in the EC dysfunction in AD.

We have established a 3D perfusable cerebral vascular model here to investigate luminal dysfunction caused by trophic factors released from brain parenchyma in AD patients. The

simplicity of only including ECs in our 3D brain vascular model allows us to identify how ECs are specifically regulated by the pathogenic Aβ released from brain parenchyma of AD patients. ECs are known to be equipped with the abluminal expression of Aβ efflux transporters such as low-density lipoprotein receptor-related protein 1 and 2 mediate elimination of Aβ from brain parenchyma to the plasma (Deane et al., 2009; Zlokovic et al., 2010). Moreover, BBB breakdown accompanying AD progression facilitates introduction of CNS secreted pathogenic Aβ peptides on the luminal side of ECs (Hartz et al., 2012).

There are several limitations remaining in this study. Here, we posit that BACEi inhibition and subsequent Aβ reduction leads to diminished endothelial activation. It is also believed that other cleavage products generated through the amyloidogenic cleavage of APP may be inhibited by BACE1 inhibition (secreted APPβ (sAPPβ), β carboxyterminal fragment (βCTF), and amino-terminal APP intracellular domain (AICD)). The effect of these fragments on the endothelium has not been studied (Chow et al., 2010; d'Uscio et al., 2017; Ristori et al., 2020) and was not examined here. This should be evaluated in future studies to better understand the effect of other APP cleavage products on endothelial cell function. In addition to Aβ 1–40 and Aβ 1–42, truncated fragments of Aβ such 4–40 and 4–42, may also be contributing to the EC activation we observed. Further work to interrogate which fragments of Aβ specifically drive EC activation, would be beneficial in expanding our understanding of Aβ mediated vascular activation. Furthermore, although we have only investigated paracrine signaling from cortical neurons with APPSwe mutation, investigation of CM obtained from BBB relevant cell types like astrocytes and microglia could provide an extensive understanding of the role of other CNS cell types in AD vascular dysfunction. While we utilized the FAD APPSwe mutation, 90% of AD patients are suffering from a sporadic form of the disease and FAD is rare. Genetic studies of SAD have identified approximately two dozen associated candidate genes (Knupp et al., 2020; Ristori et al., 2020). Incorporating these genes into the model described here could help advance our understanding of vascular changes in sporadic AD. Finally, future studies should incorporate all relevant cell types present in the BBB. Building a comprehensive BBB model and investigating cell type specific effects on the endothelium will lead to an in-depth understanding of how cerebrovascular dysfunction occurs in AD patients.

4. Methods

4.1. Endothelial cell culture

Human brain microvascular endothelial cells (HBMECs) (CC# ACBRI 376 V; Cell systems) at passage number 3–6 were used for all experiments. HBMECs were maintained in culture flasks coated with Attachment Factor (CC# 4Z0-210; cell systems) and fed growth medium (GM) (CC# 3202; EGM-2 MV Microvascular Endothelial Cell Growth Medium-2 BulletKit (CC# 3156; EBM-2 Basal Medium), 5% fetal bovine serum (FBS), hydrocortisone, human fibroblast growth factor-beta (hFGF-B), vascular endothelial growth factor (VEGF), R3-insulin-like growth factor-1 (R3-IGF-1), ascorbic acid, human epidermal growth factor (hEGF), GA-1000 (gentamycin and amphotericin)). Cells were maintained at 37 °C in a 5% CO2 incubator and media was replaced every 3 days.

4.2. Cell lines and hiPSC neuronal differentiation

To generate AD mimicking neurons from hiPSCs we used previously established gene-edited hiPSC lines heterozygous ($Swe^{+/WT}$) and homozygous ($Swe^{+/+}$) for the APP Swedish mutation as well as the parental control ($Swe^{WT/WT}$) described in Young et al. (Young et al., 2018). These cell lines were generated from a previously published and characterized CV background human induced pluripotent stem cell line (Knupp et al., 2020). This is a male cell line with an APOE ε3/ε4 genotype (Levy et al., 2007). A previously published APP knockout (APP^{KO}) line was used as an additional control for conditioned media (CM) experiments (Young et al., 2018). This cell line was made from a parental APP duplication hiPSC line and was engineered using CRISPR/Cas9 genome editing to lack APP production. Neurons from these cell lines were differentiated from hiPSCs using dual-SMAD inhibition techniques as previously described (Knupp et al., 2020; Rose et al., 2018). For the experiments presented here, we started with neural precursor cells (NPCs) previously differentiated from hiPSCs and frozen. NPCs for all the APPSwe lines ($Swe^{+/WT}$, $Swe^{+/+}$, $Swe^{WT/WT}$) and the APP^{KO} line were thawed and plated on a Matrigel (Growth factor reduced basement membrane matrix; CC# 356231; Corning) coated 6-well plates. NPCs were cultured in Basal Neural Maintenance Media (BNMM) + FGF (1:1 DMEM/F12 + Glutamine (CC# 11320–033; Gibco) and Neurobasal media (CC# 21103–049; Gibco), 0.5% N2 Supplement (CC# 17502–048; Gibco), 1% B27 Supplement (CC# 17504–044; Gibco), 0.5% GlutaMax (CC# 35050061; Thermo Fisher Scientific), 0.5% insulin-transferrin−selenium (CC# 41400045; Thermo Fisher Scientific), 0.5% NEAA (CC# 11140050; Thermo Fisher Scientific), 0.2% b-mercaptoethanol (CC# 21985023, Life Technologies) + 20 ng/mL FGF (R&D Systems, Minneapolis, MN)). The NPCs were allowed to reach 70% confluence for 1–3 days with media changes every other day. Once the NPCs were sufficiently confluent, cells were dissociated with Accutase (CC# 07930, STEMCELL Technologies) and passaged into Matrigel-coated 10 cm culture plates for neural differentiation. 24 h after replating, the cells were switched to Neural Differentiation media (BNMM +0.2 mg/mL brain-derived neurotrophic factor (CC# 450–02; PeproTech) + 0.2 mg/mL glial-cell-derived neurotrophic factor (CC# 450–10; PeproTech) + 0.5 M dbcAMP (CC# D0260; Sigma Aldrich). Media was changed twice a week for 21 days at which point the differentiation is considered finished. Cells were maintained at 37 °C in a 5% CO2 incubator.

4.3. Conditioned media preparation

Following 21 days of differentiation, Neural Differentiation media was refreshed and was then kept on the cells for at least 72 h with no media change to generate conditioned media (CM) for 2D and 3D treatment experiments. After 72 h, the media was collected and stored at 4 °C for short-term storage and −20 °C for long-term storage. To generate CM from BACEi treated APPSwe neurons, neurons were dissociated from 10 cm plates using Accutase following 21 days of differentiation and split into 3 wells of a Matrigel-coated 6 well plate. This was repeated for all cell lines. At least 3 days later, neurons were treated with either 25 nM β-secretase inhibitor (CC# HY-13240; BACEi LY2886721; MedChemExpress) or dimethyl sulfoxide (DMSO, as vehicle control) or left untreated every 24 h 72 h with no media change. After 72 h of treatment, media from untreated, DMSO, and

BACEi treated neurons was harvested for perfusion through microvessels, treatment in 2D, and quantification of Aβ1-40 and Aβ1-42 peptides secreted by neurons.

4.4. Immunoprecipitation of Aβ

For immunoprecipitation of Aβ from our CM, 4 μg/mL of mouse anti-Aβ 6E10 antibody (CC# 803001, BioLegend) was added to CM samples from the $Swe^{+/+}$ and $Swe^{WT/WT}$ lines as previously described (Dewji et al., 2006; Oberstein et al., 2021; Welzel et al., 2014). Media containing the antibody was incubated tilting, overnight at 4 °C. 50 μl of M-280 Sheep Anti-Mouse IgG Dynabeads™ (CC# 11202D, Invitrogen) for every 4 μg of antibody were added to each CM sample according to the manufacturer's instructions and the samples were incubated tilting at 4 °C for 1 h. The Dynabeads™ covalently coupled to 6E10 labeled Aβ were removed from the media using a magnet according to the manufacturer's instructions. Supernatant was removed from the magnetically separated beads and CM lacking Aβ was collected and stored at −80 °C for downstream analysis and perfusion through engineered microvessels.

4.5. Amyloid beta measurements

Aβ1-40 and Aβ1-42 peptides were measured using the methods previously described by Young et al., 2015. (Young et al., 2015) Conditioned media collected from the $Swe^{+/+}$, $Swe^{+/WT}$, $Swe^{WT/WT}$, and APP^{KO} cell lines after a 3-week differentiation were frozen at −80 °C until use. The media was run on an Aβ Triplex ELISA plate (CC# 151200E-2; MesoScale Diagnostics).

4.6. Meso-Scale Discovery (MSD) U-PLEX platform to measure extracellular levels of cytokines and chemokines

Pro-inflammatory proteins in the media were measured using the MSD U-PLEX platform (MesoScale Diagnostics). For this assay, conditioned media collected from the $Swe^{+/+}$, $Swe^{+/WT}$, $Swe^{WT/WT}$, and APP^{KO} cell lines after a 3-week differentiation were frozen at −80 °C until use. 25 μl of media was used to run an MSD U-plex assay as per manufacturer's protocol and MSD Quick plex SQ120 instrument was used to detect analytes. This MSD U-Plex plate detected a panel of pro-inflammatory cytokines including IL-1β, IL-6, IL-8, IFN-β, TNF-α, IL-15, IFN-α2a and chemokines including Eotaxin, and IP-10, known to be elevated in AD patients.

4.7. Total and phospho-tau measurements

Samples were prepared by plating differentiated neurons from the $Swe^{+/WT}$, $Swe^{+/+}$, $Swe^{WT/WT}$ and APP^{KO} lines in a 96 well plate at 300,000 cells per well. Conditioned media and cell lysate were harvested and pooled from six wells per line. Conditioned media was incubated on the cells for at least 72 h prior to collection. pTau (Thr231) and tTau levels were measured in these samples using pTAUThr231/tTAU ELISA plates (CC# K15121D-1, Meso Scale Discovery).

4.8. 3D cerebral microvessel fabrication

Engineered microvessels were fabricated using soft lithography and injection molding techniques previously described by Zheng et al., 2012. Briefly, type I rat tail collagen was dissolved in 0.1% acetic acid at a stock concentration of 15 mg/mL (Zheng et al., 2012). The collagen was neutralized and diluted to 7.5 mg/mL on ice with 1 M NaOH (20 mM final), 10× M199 (CC# 11825015; Thermo Fisher Scientific), and GM. A microfabricated polydimethylsiloxane (PDMS) stamp was used to define a double-grid vessel network with a feature height of 150 μm. Collagen was molded around this PDMS stamp. A flat collagen gel was also generated. After gelation at 37 °C, the channels were incubated with the flat collagen gel to generate closed off microchannels that can be perfused and seeded with endothelial cells (ECs). These two gels merged through additive bonding upon incubation at 37 °C. Once the gel was fabricated, HBMECs were lifted from culture flasks with trypsin (CC# MT-25-052-CI; Thermo Fisher Scientific) and resuspended in GM at a concentration of 7–10 × 10^6 cells/mL. Using a gel loading pipette tip, 10 μL of this cell suspension is injected into the inlet of the microvessel and allowing them to circumferentially attach to the collagen gel under static conditions for 1 h prior to the start of gravity-driven flow. Microvessel constructs were cultured under gravity-driven flow for 5–7 days with media replenishment approximately every 12 h.

4.9. Conditioned media treatment

For the treatment of HBMECs with CM in 2D, HBMECs were plated at a density of 0.03 M/well in a glass bottom chamber slide (CC# 80827, Ibidi) and allowed to recover for 48 h prior to treatment. Prior to treatment, the cells were washed with EBM-2 basal media (serum-free) for 5 mins. Then, 250 μL of CM per well was then added to the cells for 8 h, following which the cells were fixed in 4% PFA. To treat our engineered microvessels in 3D, vessel fabrication was performed as described above. Following vessel fabrication and culture for 5–7 days under gravity-driven flow, the vessels were treated with CM from all of our APPSwe lines and CM from BACEi treated neurons. Vessels were washed with EBM-2 basal media (serum-free) for 20 mins. Vessels were then perfused with CM for 1 h. Media was replenished every 20 mins to continue gravity-driven flow throughout the duration of treatment. Following 1 h of perfusion, the vessels were fixed with 4%PFA for 20 mins for downstream analysis and washed with phosphate buffered saline (PBS) three times for 20 mins each. For RNAseq analysis, vessels were treated for 8 h with media replenished every 2 h.

4.10. RNA isolation and RNAseq analysis

RNA was collected from two different culture subtypes (2D cultures and 3D microvessels) for three different media conditions (unconditioned BNMN media, conditioned control media and conditioned $Swe^{+/+}$ media). RNA from 2D cultures was collected following media treatment from 24 well plates by addition of RLT lysis buffer and pipette homogenization. RNA from 3D vessels was collected by perfusion of RLT lysis buffer in the inlets and collection of the lysates in the outlets. Lysates from three wells in 2D cultures were pooled as one sample replicate, and two vessels from 3D cultures were pooled as one replicate. Total RNA was isolated from the lysate using on-column digestion of genomic

DNA *via* RNeasy Micro Kit (CC# 74004; Qiagen). RNA quality was assessed using High sensitivity RNA TapeStation 4200 (Agilent Technologies) and total RNA samples with RNA integrity number > 8 were used to proceed to library preparation. For sequencing, cDNA preparation was performed using Takara SMART-Seq v4 Ultra Low Input RNA Kit (SMARTv4), library preparation using Illumina Nextera XT DNA Library Prep Kit (Nextera XT) and sequenced with Illumina NovaSeq 6000 (paired-end 50 cycles). Sequenced reads were aligned using STAR2 aligner and gene-level raw counts was obtained using STAR2's internal quantification method. Gene ontology analysis was performed using iDEP.951 for pathway analysis of differentially expressed genes.

4.11. Isolated platelet and peripheral blood mononuclear cell (PBMC) perfusion in microvessels

Whole blood was drawn from normal healthy donors into a blood collection tube (BD, CC# 364606; Vacutainer) containing 1.5 mL of acid citrate dextrose (ACD). Platelets were isolated from whole blood using an existing protocol provided by the manufacturer. Briefly, collected blood was centrifuged at 200 *g* for 20 min (acceleration 4; deceleration 0) at room temperature for platelet-rich plasma (PRP) extraction. PRP was subsequently centrifuged at 1200 *g* for 10 min to obtain pellets containing the isolated platelets. Pellets were resuspended in CGS buffer containing 120 mM NaCl, 13 mM Sodium Citrate and 30 mM Glucose supplemented with Prostaglandin E1 (sigma P5515-1MG) at 1:10,000 (vol: vol) to inhibit aggregation of platelets. Isolated platelets rinsed in CGS/PGE1 buffer were counted under a bright-field microscope using a hemocytometer and centrifuged again using the previous setting. Pellets were resuspended carefully in Tyrode's buffer containing 5.5 mM glucose, 10 mM HEPES, 138 mM NaCl, 12 mm HaHCO3, 2.9 mM KCL and 0.36 mM NaH2PO4 and stained with CD41a (CC# 555467; BD) conjugated with phycoerythrin (PE) for 30 min. Following staining, platelet concentration was adjusted to 5 × 10^7 platelets/mL by supplementing an additional Tyrode's buffer.

Isolated platelets were perfused in conditioned media treated microvessels to assess the functional activation of endothelial cells. CD41a labeled isolated platelets were perfused in HBMEC microvessels treated with conditioned media for 1 h through transfer pipettes to avoid shear-induced activation. Approximately 150 μl of platelets resuspended in Tyrode's buffer was pipetted into the inlets of microvessels and incubated at 37C for 20 min. Following platelet treatment, vessels were washed three times, each rinse for five minutes, to eliminate residual unbound platelets within the vessel lumen. Immediately after the wash step, microvessels were fixed in 4% paraformaldehyde solution and rinsed with PBS three times. Platelet adhesion analysis was performed after performing immunofluorescent staining of VWF and confocal imaging.

PBMCs were also isolated from freshly drawn blood samples collected in ACD blood collection tube (BD CC# 364606; Vacutainer). PBMCs were isolated using density gradient centrifugation in a 50 mL SepMate tube (StemCell Technologies) following manufacturer's protocol. PBMCs were stained with pan-leukocyte marker CD45 (CC# 555485; BD biosciences) for live imaging of leukocyte adhesion on $Swe^{+/+}$ CM treated HBMEC microvessel for 1 h.

4.12. Scanning electron microscopy imaging of platelet bound VWF fibers

Swe$^{+/+}$ perfused microvessels were fixed in ½ strength Karnovsky's fixative (2% paraformaldehyde and 2.5% glutaraldehyde) overnight at 4C. The top and bottom layers of the collagen matrices were gently teased apart and rinsed with 0.1 M cacodylate buffer. Samples were dehydrated with graded series of alcohols and critical point dried (Autosamdri, Tousimis Corp). Microvessel layers were sputter coated with Au/Pd alloy (Denton Desk IV, Denton Vacuum) and imaged using a JSM 6610 LV scanning electron microscope (JEOL) at an accelerating voltage of 5 kV.

4.13. Flow cytometry analysis

To characterize vascular cell adhesion molecule 1 expression on the surface of endothelial cell following CM treatment, multiparameter FACS analysis of CM treated human brain endothelial cells was performed. BD FACS Canto II was used to analyze VCAM-1 positive cells using FTIC-anti-VCAM-1 antibody (CC# ab24853; Abcam) and the number of positive cells were quantified using with FlowJo software (Tree Star). Unstained controls were used to compensate and adjust voltage.

4.14. Immunofluorescent staining and image analysis

At the end of each experimental time point, both microvessels and 2D endothelial cultures were fixed with 4% paraformaldehyde for 20 min and washed with PBS three times. For immunofluorescent staining of microvessels, reagents were perfused through the microchannels through the inlet of the acrylic jigs. PBS containing 2% bovine serum albumin (BSA) was used to block microvessels and 2D cultures for analysis of extracellular VWF. Following 1 h of blocking, FITC conjugated VWF antibody (1:100; Abcam CC# ab8822) was added to samples for 1 h at room temperature and washed three times with PBS before proceeding to stain with the remaining antibody of interest. Treatment with 2% BSA with 0.1% Triton-x preceded before staining with antibodies including CD41a (CC# 555467; BD), phalloidin (CC# A12380; Thermo Fisher), CD144 (CC# 136008; BioLegend) for cell permeabilization and blocking non-specific binding. All stained microvessels and 2D cultures were imaged using Yokogawa W1 spinning disk confocal microscope or Leica SP8 laser confocal microscope. For microvessels, the entire collagen construct was imaged using a 5 by 5 large z stack image stitch (10% blending stitch) under a 10× objective with a z-step size of 5.5 μm. 3D reconstruction and cross-sectional images of the microvessels were rendered using ImageJ software.

4.15. VWF fiber quantification

VWF fibers were quantified into two distinct wall-fiber and transluminal fiber categories. Transluminal fibers were quantified from fibers formed cross-sectionally within the microchannels and are characteristically thicker and straighter than wall fibers. Wall fibers were quantified from string fibers found circumferentially on the endothelial surface and are smaller and tortuous by nature. For classification of the number of fibers found in each group, stitched z stack Images of each vessel were divided into three layers: top, center lumen and bottom. The top and bottom layers were constructed from compilation of initial

and final 4 z-stacks (~20 μm) of each image construct respectively. The luminal layer was constructed from compiled z stack images excluding the initial and final 4 layers.

4.16. Statistical analysis

Statistical analysis of fiber quantification was performed with either one-way ANOVA or two-way ANOVA for comparison between groups followed by Tukey's or Šídák's *post hoc* test for multiple comparisons between groups. Statistical analysis on the RNAseq was conducted with Fischer's Exact test. Significance was defined as a value of $p < 0.05$. For all imaging experiments the data was analyzed in a blinded manner. Statistical analysis was performed using GraphPad Prism software. Information on statistical details of individual experiments can be found in the respective figure legends.

Supplementary Material

Refer to Web version on PubMed Central for supplementary material.

Acknowledgments

We would like to acknowledge the Lynn and Mike Garvey Imaging Laboratory in the Institute for Stem Cells and Regenerative Medicine (ISCRM) and the Flow Cytometry Core at the University of Washington. We also acknowledge the Electron Microscopy Laboratory and Genomics & Bioinformatics Laboratory both at Fred Hutchinson Cancer Research Center. We would also like to acknowledge that schematics were made using BioRender.

Funding

We acknowledge the financial support of National Institute of Health grants R21AG074373 (to Y.Z. and J.E.Y), R01AG062148 (to J.E.Y), 1R61/33HL154250 (to Y.Z.) and T32AG066574 (to K.M.E, training grant). Additionally, we acknowledge the financial support of Institute for Stem Cell and Regenerative Medicine (to Y.S., fellowship).

Data availability

All data needed to evaluate the conclusions in this paper are present in the main paper and/or the Supplementary Materials. Additional data related to this paper may be requested from the corresponding author.

Abbreviations:

APPSwe	amyloid precursor protein Swedish mutation
CM	conditioned media
HBMEC	human brain microvascular endothelial cell
WPB	Weibel-Palade bodies
hiPSCs	human induced pluripotent stem cells
BACE1	β-secretase 1
BACEi	β-secretase 1 inhibitor
hiPSC-CNs	human induced pluripotent stem cell derived cortical neurons

APP^{KO}	APP knock out
$Swe^{+/+}$	homozygous for APP Swedish mutation
Swe $^{+/WT}$	heterozygous for APP Swedish mutation
$Swe^{WT/WT}$	isogenic control for APP Swedish mutation
CNs	cortical neurons
UCM	unconditioned media

References

2021 Alzheimer''s disease facts and figures, 2021. Alzheimers Dement. 17, 327–406. 10.1002/alz.12328. [PubMed: 33756057]

Behl T, Kaur I, Fratila O, Brata R, Bungau S, 2020. Exploring the potential of therapeutic agents targeted towards mitigating the events associated with amyloid-β cascade in Alzheimer's disease. Int. J. Mol. Sci 21 10.3390/ijms21207443.

Behl T, Kaur I, Sehgal A, Singh S, Albarrati A, Albratty M, Najmi A, Meraya AM, Bungau S, 2022. The road to precision medicine: eliminating the "one size fits all" approach in Alzheimer's disease. Biomed. Pharmacother. 153, 113337 10.1016/j.biopha.2022.113337. [PubMed: 35780617]

Bhatia R, Lin H, Lal R, 2000. Fresh and globular amyloid β protein (1–42) induces rapid cellular degeneration: evidence for AβP channel-mediated cellular toxicity. FASEB J 14, 1233–1243. 10.1096/fasebj.14.9.1233. [PubMed: 10834945]

Blanchard JW, Bula M, Davila-Velderrain J, Akay LA, Zhu L, Frank A, Victor MB, Bonner JM, Mathys H, Lin Y-T, Ko T, Bennett DA, Cam HP, Kellis M, Tsai L-H, 2020. Reconstruction of the human blood–brain barrier in vitro reveals a pathogenic mechanism of APOE4 in pericytes. Nat. Med 26, 952–963. 10.1038/s41591-020-0886-4. [PubMed: 32514169]

Borroni B, Volpi R, Martini G, Del Bono R, Archetti S, Colciaghi F, Akkawi NM, Di Luca M, Romanelli G, Caimi L, Padovani A, 2002. Peripheral blood abnormalities in Alzheimer disease: evidence for early endothelial dysfunction. Alzheimer Dis. Assoc. Disord. 16.

Brookmeyer R, Johnson E, Ziegler-Graham K, Arrighi HM, 2007. Forecasting the global burden of Alzheimer's disease. Alzheimers Dement. 3, 186–191. 10.1016/j.jalz.2007.04.381. [PubMed: 19595937]

Chen S-C, Huang C-C, Chien C-L, Jeng C-J, Su H-T, Chiang E, Liu M-R, Wu CHH, Chang C-N, Lin R-H, 2004. Cross-linking of P-selectin glycoprotein ligand-1 induces death of activated T cells. Blood 104, 3233–3242. 10.1182/blood-2003-05-1679. [PubMed: 15198951]

Chen MB, Yang AC, Yousef H, Lee D, Chen W, Schaum N, Lehallier B, Quake SR, Wyss-Coray T, 2020. Brain endothelial cells are exquisite sensors of age-related circulatory cues. Cell Rep. 30, 4418–4432.e4. 10.1016/j.celrep.2020.03.012. [PubMed: 32234477]

Choublier N, Taghi M, Menet M-C, Le Gall M, Bruce J, Chafey P, Guillonneau F, Moreau A, Denizot C, Parmentier Y, Nakib S, Borderie D, Bouzinba-Segard H, Couraud P-O, Bourdoulous S, Declèves X, 2022. Exposure of human cerebral microvascular endothelial cells hCMEC/D3 to laminar shear stress induces vascular protective responses. Fluids Barriers CNS 19, 41. 10.1186/s12987-022-00344-w. [PubMed: 35658915]

Chow VW, Mattson MP, Wong PC, Gleichmann M, 2010. An overview of APP processing enzymes and products. NeuroMolecular Med 12, 1–12. 10.1007/s12017-009-8104-z. [PubMed: 20232515]

Chui R, Dorovini-Zis K, 2010. Regulation of CCL2 and CCL3 expression in human brain endothelial cells by cytokines and lipopolysaccharide. J. Neuroinflammation 7, 1. 10.1186/1742-2094-7-1. [PubMed: 20047691]

Cleator JH, Zhu WQ, Vaughan DE, Hamm HE, 2006. Differential regulation of endothelial exocytosis of P-selectin and von Willebrand factor by protease-activated receptors and cAMP. Blood 107, 2736–2744. 10.1182/blood-2004-07-2698. [PubMed: 16332977]

Cook-Mills JM, Marchese ME, Abdala-Valencia H, 2010. Vascular cell adhesion molecule-1 expression and signaling during disease: regulation by reactive oxygen species and antioxidants. Antioxid. Redox Signal. 15, 1607–1638. 10.1089/ars.2010.3522.

Cucullo L, Couraud P-O, Weksler B, Romero I-A, Hossain M, Rapp E, Janigro D, 2007. Immortalized human brain endothelial cells and flow-based vascular modeling: a marriage of convenience for rational neurovascular studies. J. Cereb. Blood Flow Metab 28, 312–328. 10.1038/sj.jcbfm.9600525. [PubMed: 17609686]

Deane R, Bell RD, Sagare A, Zlokovic BV, 2009. Clearance of amyloid-beta peptide across the blood-brain barrier: implication for therapies in Alzheimer's disease. CNS Neurol. Disord. Drug Targets 8, 16–30. 10.2174/187152709787601867. [PubMed: 19275634]

DeTure MA, Dickson DW, 2019. The neuropathological diagnosis of Alzheimer's disease. Mol. Neurodegener. 14, 32. 10.1186/s13024-019-0333-5. [PubMed: 31375134]

Dewji NN, Mukhopadhyay D, Singer SJ, 2006. An early specific cell-cell interaction occurs in the production of β-amyloid in cell cultures. Proc. Natl. Acad. Sci 103, 1540–1545. 10.1073/pnas.0509899103. [PubMed: 16432203]

Drakeford C, O'Donnell JS, 2017. Targeting von Willebrand factor–mediated inflammation. Arterioscler. Thromb. Vasc. Biol 37, 1590–1591. 10.1161/ATVBAHA.117.309817. [PubMed: 28835483]

d'Uscio LV, He T, Katusic ZS, 2017. Expression and processing of amyloid precursor protein in vascular endothelium. Physiology (Bethesda) 32, 20–32. 10.1152/physiol.00021.2016. [PubMed: 27927802]

Fonseca ACRG, Moreira PI, Oliveira CR, Cardoso SM, Pinton P, Pereira CF, 2015. Amyloid-beta disrupts calcium and redox homeostasis in brain endothelial cells. Mol. Neurobiol. 51, 610–622. 10.1007/s12035-014-8740-7. [PubMed: 24833600]

Fu H, Jiang Y, Yang D, Scheiflinger F, Wong WP, Springer TA, 2017. Flow-induced elongation of von Willebrand factor precedes tension-dependent activation. Nat. Commun. 8, 324. 10.1038/s41467-017-00230-2. [PubMed: 28831047]

Gate D, Saligrama N, Leventhal O, Yang AC, Unger MS, Middeldorp J, Chen K, Lehallier B, Channappa D, De Los Santos MB, McBride A, Pluvinage J, Elahi F, Tam GK-Y, Kim Y, Greicius M, Wagner AD, Aigner L, Galasko DR, Davis MM, Wyss-Coray T, 2020. Clonally expanded CD8 T cells patrol the cerebrospinal fluid in Alzheimer's disease. Nature 577, 399–404. 10.1038/s41586-019-1895-7. [PubMed: 31915375]

Govindpani K, McNamara LG, Smith NR, Vinnakota C, Waldvogel HJ, Faull RL, Kwakowsky A, 2019. Vascular dysfunction in Alzheimer's disease: a prelude to the pathological process or a consequence of it? J. Clin. Med 8 10.3390/jcm8050651.

Grammas P, 2011. Neurovascular dysfunction, inflammation and endothelial activation: implications for the pathogenesis of Alzheimer's disease. J. Neuroinflammation 8, 26. 10.1186/1742-2094-8-26. [PubMed: 21439035]

Guerreiro R, Bras J, 2015. The age factor in Alzheimer's disease. Genom. Med 7, 106. 10.1186/s13073-015-0232-5.

Gupta A, Watkins A, Thomas P, Majer R, Habubi N, Morris G, Pansari K, 2005. Coagulation and inflammatory markers in Alzheimer's and vascular dementia. Int. J. Clin. Pract 59, 52–57. 10.1111/j.1742-1241.2004.00143.x. [PubMed: 15707465]

Haass C, Lemere CA, Capell A, Citron M, Seubert P, Schenk D, Lannfelt L, Selkoe DJ, 1995. The Swedish mutation causes early-onset Alzheimer's disease by β-secretase cleavage within the secretory pathway. Nat. Med 1, 1291–1296. 10.1038/nm1295-1291. [PubMed: 7489411]

Hansson O, Lehmann S, Otto M, Zetterberg H, Lewczuk P, 2019. Advantages and disadvantages of the use of the CSF amyloid β (Aβ) 42/40 ratio in the diagnosis of Alzheimer's disease. Alzheimers Res. Ther 11, 34. 10.1186/s13195-019-0485-0. [PubMed: 31010420]

Hartz AMS, Bauer B, Soldner ELB, Wolf A, Boy S, Backhaus R, Mihaljevic I, Bogdahn U, Klünemann HH, Schuierer G, Schlachetzki F, 2012. Amyloid-β contributes to blood-brain barrier leakage in transgenic human amyloid precursor protein mice and in humans with cerebral amyloid angiopathy. Stroke 43, 514–523. 10.1161/STROKEAHA.111.627562. [PubMed: 22116809]

Helle E, Ampuja M, Antola L, Kivelä R, 2020. Flow-induced transcriptomic remodeling of endothelial cells derived from human induced pluripotent stem cells. Front. Physiol 11, 591450. 10.3389/fphys.2020.591450. [PubMed: 33178051]

Janelidze S, Stomrud E, Palmqvist S, Zetterberg H, van Westen D, Jeromin A, Song L, Hanlon D, Tan Hehir CA, Baker D, Blennow K, Hansson O, 2016. Plasma β-amyloid in Alzheimer's disease and vascular disease. Sci. Rep 6, 26801. 10.1038/srep26801. [PubMed: 27241045]

Järemo P, Milovanovic M, Buller C, Nilsson S, Winblad B, 2013. P-selectin paradox and dementia of the Alzheimer type: circulating P-selectin is increased but platelet-bound P-selectin after agonist provocation is compromised. Scand. J. Clin. Lab. Invest 73, 170–174. 10.3109/00365513.2013.764572. [PubMed: 23421771]

Kass B, Schemmert S, Zafiu C, Pils M, Bannach O, Kutzsche J, Bujnicki T, Willbold D, 2022. Aβ oligomer concentration in mouse and human brain and its drug-induced reduction ex vivo. Cell. Rep. Med 3, 100630 10.1016/j.xcrm.2022.100630. [PubMed: 35584626]

Kelleher RJ, Soiza RL, 2013. Evidence of endothelial dysfunction in the development of Alzheimer's disease: is Alzheimer's a vascular disorder? Am. J. Cardiovasc. Dis 3, 197–226. [PubMed: 24224133]

Knupp A, Mishra S, Martinez R, Braggin JE, Szabo M, Kinoshita C, Hailey DW, Small SA, Jayadev S, Young JE, 2020. Depletion of the AD risk gene SORL1 selectively impairs neuronal endosomal traffic independent of amyloidogenic APP processing. Cell Rep 31, 107719 10.1016/j.celrep.2020.107719. [PubMed: 32492427]

Kook S-Y, Hong HS, Moon M, Ha CM, Chang S, Mook-Jung I, 2012. Aβ1-42-RAGE interaction disrupts tight junctions of the blood–brain barrier via Ca2+-calcineurin signaling. J. Neurosci 32, 8845–8854. 10.1523/JNEUROSCI.6102-11.2012. [PubMed: 22745485]

Kuchibhotla KV, Wegmann S, Kopeikina KJ, Hawkes J, Rudinskiy N, Andermann ML, Spires-Jones TL, Bacskai BJ, Hyman BT, 2014. Neurofibrillary tangle-bearing neurons are functionally integrated in cortical circuits in vivo. Proc. Natl. Acad. Sci 111, 510–514. 10.1073/pnas.1318807111. [PubMed: 24368848]

Lee W-J, Liao Y-C, Wang Y-F, Lin I-F, Wang S-J, Fuh J-L, 2018. Plasma MCP-1 and cognitive decline in patients with Alzheimer's disease and mild cognitive impairment: a two-year follow-up study. Sci. Rep 8, 1280. 10.1038/s41598-018-19807-y. [PubMed: 29352259]

Levy S, Sutton G, Ng PC, Feuk L, Halpern AL, Walenz BP, Axelrod N, Huang J, Kirkness EF, Denisov G, Lin Y, MacDonald JR, Pang AWC, Shago M, Stockwell TB, Tsiamouri A, Bafna V, Bansal V, Kravitz SA, Busam DA, Beeson KY, McIntosh TC, Remington KA, Abril JF, Gill J, Borman J, Rogers Y-H, Frazier ME, Scherer SW, Strausberg RL, Venter JC, 2007. The diploid genome sequence of an individual human. PLoS Biol 5, e254. [PubMed: 17803354]

Lim YY, Maruff P, Kaneko N, Doecke J, Fowler C, Villemagne VL, Kato T, Rowe CC, Arahata Y, Iwamoto S, Ito K, Tanaka K, Yanagisawa K, Masters CL, Nakamura A, 2020. Plasma amyloid-β biomarker associated with cognitive decline in preclinical Alzheimer's disease. J. Alzheimers Dis 77, 1057–1065. 10.3233/JAD-200475. [PubMed: 32925048]

Lip GYH, Blann A, 1997a. von Willebrand factor: a marker of endothelial dysfunction in vascular disorders? Cardiovasc. Res 34, 255–265. 10.1016/S0008-6363(97)00039-4. [PubMed: 9205537]

Lip GYH, Blann A, 1997b. von Willebrand factor: a marker of endothelial dysfunction in vascular disorders? Cardiovasc. Res 34, 255–265. 10.1016/S0008-6363(97)00039-4. [PubMed: 9205537]

Mehta PD, Pirttilä T, Mehta SP, Sersen EA, Aisen PS, Wisniewski HM, 2000. Plasma and cerebrospinal fluid levels of amyloid β proteins 1–40 and 1–42 in Alzheimer disease. Arch. Neurol 57, 100–105. 10.1001/archneur.57.1.100. [PubMed: 10634455]

Michaux G, Cutler DF, 2004. How to roll an endothelial cigar: the biogenesis of Weibel-Palade bodies. Traffic 5, 69–78. 10.1111/j.1600-0854.2004.00157.x. [PubMed: 14690496]

Mietkowska M, Schuberth C, Wedlich-Söldner R, Gerke V, 2019. Actin dynamics during Ca(2+)-dependent exocytosis of endothelial Weibel-Palade bodies. Biochim. Biophys. Acta, Mol. Cell Res 1866, 1218–1229. 10.1016/j.bbamcr.2018.11.010. [PubMed: 30465794]

Na H-J, Yeum CE, Kim H-S, Lee J, Kim JY, Cho YS, 2019. TSPYL5-mediated inhibition of p53 promotes human endothelial cell function. Angiogenesis 22, 281–293. 10.1007/s10456-018-9656-z. [PubMed: 30471052]

Nakamura A, Kaneko N, Villemagne VL, Kato T, Doecke J, Doré V, Fowler C, Li Q-X, Martins R, Rowe C, Tomita T, Matsuzaki K, Kenji Ishii, Kazunari Ishii, Arahata Y, Iwamoto S, Ito K, Tanaka K, Masters CL, Yanagisawa K, 2018. High performance plasma amyloid-β biomarkers for Alzheimer's disease. Nature 554, 249–254. 10.1038/nature25456. [PubMed: 29420472]

Oberstein TJ, Utz J, Spitzer P, Klafki HW, Wiltfang J, Lewczuk P, Kornhuber J, Maler JM, 2021. The role of Cathepsin B in the degradation of Aβ and in the production of Aβ peptides starting with Ala2 in cultured astrocytes. Front. Mol. Neurosci 13 10.3389/fnmol.2020.615740.

Park J, Wetzel I, Marriott I, Dréau D, D'Avanzo C, Kim DY, Tanzi RE, Cho H, 2018. A 3D human triculture system modeling neurodegeneration and neuroinflammation in Alzheimer's disease. Nat. Neurosci 21, 941–951. 10.1038/s41593-018-0175-4. [PubMed: 29950669]

Parodi-Rullán R, Sone JY, Fossati S, 2019. Endothelial mitochondrial dysfunction in cerebral amyloid angiopathy and Alzheimer's disease. J. Alzheimers Dis 72, 1019–1039. 10.3233/JAD-190357. [PubMed: 31306129]

Peng Z, Shu B, Zhang Y, Wang M, 2019. Endothelial response to pathophysiological stress. Arterioscler. Thromb. Vasc. Biol 39, e233–e243. 10.1161/ATVBAHA.119.312580. [PubMed: 31644356]

Penney J, Ralvenius WT, Tsai L-H, 2020a. Modeling Alzheimer's disease with iPSC-derived brain cells. Mol. Psychiatry 25, 148–167. 10.1038/s41380-019-0468-3. [PubMed: 31391546]

Penney J, Ralvenius WT, Tsai L-H, 2020b. Modeling Alzheimer's disease with iPSC-derived brain cells. Mol. Psychiatry 25, 148–167. 10.1038/s41380-019-0468-3. [PubMed: 31391546]

Petri B, Broermann A, Li H, Khandoga AG, Zarbock A, Krombach F, Goerge T, Schneider SW, Jones C, Nieswandt B, Wild MK, Vestweber D, 2010. von Willebrand factor promotes leukocyte extravasation. Blood 116, 4712–4719. 10.1182/blood-2010-03-276311. [PubMed: 20716766]

Propson NE, Roy ER, Litvinchuk A, Köhl J, Zheng H, 2021. Endothelial C3a receptor mediates vascular inflammation and blood-brain barrier permeability during aging. J. Clin. Invest 131 10.1172/JCI140966.

Redd MA, Zeinstra N, Qin W, Wei W, Martinson A, Wang Y, Wang RK, Murry CE, Zheng Y, 2019. Patterned human microvascular grafts enable rapid vascularization and increase perfusion in infarcted rat hearts. Nat. Commun. 10, 584. 10.1038/s41467-019-08388-7. [PubMed: 30718840]

Ringman JM, Sachs MC, Zhou Y, Monsell SE, Saver JL, Vinters HV, 2014. Clinical predictors of severe cerebral amyloid angiopathy and influence of APOE genotype in persons with pathologically verified Alzheimer disease. JAMA Neurol 71, 878–883. 10.1001/jamaneurol.2014.681. [PubMed: 24797962]

Rissman RA, Trojanowski JQ, Shaw LM, Aisen PS, 2012. Longitudinal plasma amyloid beta as a biomarker of Alzheimer's disease. J. Neural Transm 119, 843–850. 10.1007/s00702-012-0772-4. [PubMed: 22354745]

Ristori E, Donnini S, Ziche M, 2020. New insights into blood-brain barrier maintenance: the homeostatic role of β-amyloid precursor protein in cerebral vasculature. Front. Physiol 11, 1056. 10.3389/fphys.2020.01056. [PubMed: 32973564]

Rose SE, Frankowski H, Knupp A, Berry BJ, Martinez R, Dinh SQ, Bruner LT, Willis SL, Crane PK, Larson EB, Grabowski T, Darvas M, Keene CD, Young JE, 2018. Leptomeninges-derived induced pluripotent stem cells and directly converted neurons from autopsy cases with varying neuropathologic backgrounds. J. Neuropathol. Exp. Neurol 77, 353–360. 10.1093/jnen/nly013. [PubMed: 29474672]

Satir TM, Agholme L, Karlsson A, Karlsson M, Karila P, Illes S, Bergström P, Zetterberg H, 2020. Partial reduction of amyloid β production by β-secretase inhibitors does not decrease synaptic transmission. Alzheimers Res. Ther 12, 63. 10.1186/s13195-020-00635-0. [PubMed: 32456694]

Schaum N, Lehallier B, Hahn O, Pálovics R, Hosseinzadeh S, Lee SE, Sit R, Lee DP, Losada PM, Zardeneta ME, Fehlmann T, Webber JT, McGeever A, Calcuttawala K, Zhang H, Berdnik D, Mathur V, Tan W, Zee A, Tan M, Almanzar N, Antony J, Baghel AS, Bakerman I, Bansal I, Barres BA, Beachy PA, Berdnik D, Bilen B, Brownfield D, Cain C, Chan CKF, Chen MB, Clarke MF, Conley SD, Darmanis S, Demers A, Demir K, de Morree A, Divita T, du Bois H, Ebadi H, Espinoza FH, Fish M, Gan Q, George BM, Gillich A, Gòmez-Sjöberg R, Green F, Genetiano G, Gu X, Gulati GS, Hahn O, Haney MS, Hang Y, Harris L, He M, Hosseinzadeh S, Huang A, Huang KC, Iram T, Isobe T, Ives F, Jones R, Kao KS, Karkanias J, Karnam G, Keller A,

Kershner AM, Khoury N, Kim SK, Kiss BM, Kong W, Krasnow MA, Kumar ME, Kuo CSY, Lam J, Lee DP, Lee SE, Lehallier B, Leventhal O, Li G, Li Q, Liu L, Lo A, Lu W-J, Lugo-Fagundo MF, Manjunath A, May AP, Maynard A, McGeever A, McKay M, McNerney MW, Merrill B, Metzger RJ, Mignardi M, Min D, Nabhan AN, Neff NF, Ng KM, Nguyen PK, Noh J, Nusse R, Pálovics R, Patkar R, Peng WC, Penland L, Pisco AO, Pollard K, Puccinelli R, Qi Z, Quake SR, Rando TA, Rulifson EJ, Schaum N, Segal JM, Sikandar SS, Sinha R, Sit RV, Sonnenburg J, Staehli D, Szade K, Tan M, Tan W, Tato C, Tellez K, Dulgeroff LBT, Travaglini KJ, Tropini C, Tsui M, Waldburger L, Wang BM, van Weele LJ, Weinberg K, Weissman IL, Wosczyna MN, Wu SM, Wyss-Coray T, Xiang J, Xue S, Yamauchi KA, Yang AC, Yerra LP, Youngyunpipatkul J, Yu B, Zanini F, Zardeneta ME, Zee A, Zhao C, Zhang F, Zhang H, Zhang MJ, Zhou L, Zou J, Pisco AO, Karkanias J, Neff NF, Keller A, Darmanis S, Quake SR, Wyss-Coray T, Consortium, T.T.M, 2020. Ageing hallmarks exhibit organ-specific temporal signatures. Nature 583, 596–602. 10.1038/s41586-020-2499-y. [PubMed: 32669715]

Shin Y, Choi SH, Kim E, Bylykbashi E, Kim JA, Chung S, Kim DY, Kamm RD, Tanzi RE, 2019. Blood–brain barrier dysfunction in a 3D in vitro model of Alzheimer's disease. Adv. Sci 6, 1900962. 10.1002/advs.201900962.

Spires-Jones TL, Hyman BT, 2014. The intersection of amyloid beta and tau at synapses in Alzheimer's disease. Neuron 82, 756–771. 10.1016/j.neuron.2014.05.004. [PubMed: 24853936]

Suhara T, Magrané J, Rosen K, Christensen R, Kim H-S, Zheng B, McPhie DL, Walsh K, Querfurth H, 2003. Aβ42 generation is toxic to endothelial cells and inhibits eNOS function through an Akt/GSK-3β signaling-dependent mechanism. Neurobiol. Aging 24, 437–451. 10.1016/S0197-4580(02)00135-5. [PubMed: 12600720]

Szu JI, Obenaus A, 2021. Cerebrovascular phenotypes in mouse models of Alzheimer's disease. J. Cereb. Blood Flow Metab 41, 1821–1841. 10.1177/0271678X21992462. [PubMed: 33557692]

Tietz S, Engelhardt B, 2015. Brain barriers: crosstalk between complex tight junctions and adherens junctions. J. Cell Biol 209, 493–506. 10.1083/jcb.201412147. [PubMed: 26008742]

Vidoni ED, Yeh H-W, Morris JK, Newell KL, Alqahtani A, Burns NC, Burns JM, Billinger SA, 2016. Cerebral β-amyloid Angiopathy is associated with earlier dementia onset in Alzheimer's disease. Neurodegener. Dis 16, 218–224. 10.1159/000441919. [PubMed: 26756746]

Weller RO, Preston SD, Subash M, Carare RO, 2009. Cerebral amyloid angiopathy in the aetiology and immunotherapy of Alzheimer disease. Alzheimers Res. Ther 1, 6. 10.1186/alzrt6. [PubMed: 19822028]

Welzel AT, Maggio JE, Shankar GM, Walker DE, Ostaszewski BL, Li S, Klyubin I, Rowan MJ, Seubert P, Walsh DM, Selkoe DJ, 2014. Secreted amyloid β-proteins in a cell culture model include N-terminally extended peptides that impair synaptic plasticity. Biochemistry 53, 3908–3921. 10.1021/bi5003053. [PubMed: 24840308]

Williams LM, Fujimoto T, Weaver RR, Logsdon AF, Evitts KM, Young JE, Banks WA, Erickson MA, 2022. Prolonged culturing of iPSC-derived brain endothelial-like cells is associated with quiescence, downregulation of glycolysis, and resistance to disruption by an Alzheimer's brain milieu. Fluids Barriers CNS 19, 10. 10.1186/s12987-022-00307-1. [PubMed: 35123529]

Wolters F, Boender J, Hofman A, De Maat M, Koudstaal P, Leebeek F, Ikram M, 2016. Von Willebrand factor and the risk of dementia: a population-based study (P1.092). Neurology 86.

Xu Jan, Chen S, Ku G, Ahmed SH, Jinming Xu, Chen H, Hsu CY, 2001. Amyloid β peptide–induced cerebral endothelial cell death involves mitochondrial dysfunction and caspase activation. J. Cereb. Blood Flow Metab 21, 702–710. 10.1097/00004647-200106000-00008. [PubMed: 11488539]

Yang AC, Vest RT, Kern F, Lee DP, Agam M, Maat CA, Losada PM, Chen MB, Schaum N, Khoury N, Toland A, Calcuttawala K, Shin H, Pálovics R, Shin A, Wang EY, Luo J, Gate D, Schulz-Schaeffer WJ, Chu P, Siegenthaler JA, McNerney MW, Keller A, Wyss-Coray T, 2022. A human brain vascular atlas reveals diverse mediators of Alzheimer's risk. Nature 603, 885–892. 10.1038/s41586-021-04369-3. [PubMed: 35165441]

Yau JW, Teoh H, Verma S, 2015. Endothelial cell control of thrombosis. BMC Cardiovasc. Disord 15, 130. 10.1186/s12872-015-0124-z. [PubMed: 26481314]

Young JE, Boulanger-Weill J, Williams DA, Woodruff G, Buen F, Revilla AC, Herrera C, Israel MA, Yuan SH, Edland SD, Goldstein LSB, 2015. Elucidating molecular phenotypes caused by the

SORL1 Alzheimer's disease genetic risk factor using human induced pluripotent stem cells. Cell Stem Cell 16, 373–385. 10.1016/j.stem.2015.02.004. [PubMed: 25772071]

Young JE, Fong LK, Frankowski H, Petsko GA, Small SA, Goldstein LSB, 2018. Stabilizing the retromer complex in a human stem cell model of Alzheimer's disease reduces TAU phosphorylation independently of amyloid precursor protein. Stem Cell. Rep 10, 1046–1058. 10.1016/j.stemcr.2018.01.031.

Yousef H, Czupalla CJ, Lee D, Chen MB, Burke AN, Zera KA, Zandstra J, Berber E, Lehallier B, Mathur V, Nair RV, Bonanno LN, Yang AC, Peterson T, Hadeiba H, Merkel T, Körbelin J, Schwaninger M, Buckwalter MS, Quake SR, Butcher EC, Wyss-Coray T, 2019. Aged blood impairs hippocampal neural precursor activity and activates microglia via brain endothelial cell VCAM1. Nat. Med 25, 988–1000. 10.1038/s41591-019-0440-4. [PubMed: 31086348]

Zenaro E, Pietronigro E, Bianca V. Della, Piacentino G, Marongiu L, Budui S, Turano E, Rossi B, Angiari S, Dusi S, Montresor A, Carlucci T, Nanì S, Tosadori, Calciano L, Catalucci D, Berton G, Bonetti B, Constantin, G., 2015. Neutrophils promote Alzheimer's disease–like pathology and cognitive decline via LFA-1 integrin. Nat. Med 21, 880–886. 10.1038/nm.3913. [PubMed: 26214837]

Zenaro E, Piacentino G, Constantin G, 2017. The blood-brain barrier in Alzheimer's disease. Neurobiol. Dis 107, 41–56. 10.1016/j.nbd.2016.07.007. [PubMed: 27425887]

Zheng Y, Chen J, Craven M, Choi NW, Totorica S, Diaz-Santana A, Kermani P, Hempstead B, Fischbach-Teschl C, López JA, Stroock AD, 2012. In vitro microvessels for the study of angiogenesis and thrombosis. Proc. Natl. Acad. Sci 109, 9342–9347. 10.1073/pnas.1201240109. [PubMed: 22645376]

Zheng Y, Chen J, López JA, 2015. Flow-driven assembly of VWF fibres and webs in in vitro microvessels. Nat. Commun. 6, 7858. 10.1038/ncomms8858. [PubMed: 26223854]

Zlokovic BV, Deane R, Sagare AP, Bell RD, Winkler EA, 2010. Low-density lipoprotein receptor-related protein-1: a serial clearance homeostatic mechanism controlling Alzheimer's amyloid β-peptide elimination from the brain. J. Neurochem 115, 1077–1089. 10.1111/j.1471-4159.2010.07002.x. [PubMed: 20854368]

Zuliani G, Cavalieri M, Galvani M, Passaro A, Munari MR, Bosi C, Zurlo A, Fellin R, 2008. Markers of endothelial dysfunction in older subjects with late onset Alzheimer's disease or vascular dementia. J. Neurol. Sci 272, 164–170. 10.1016/j.jns.2008.05.020. [PubMed: 18597785]

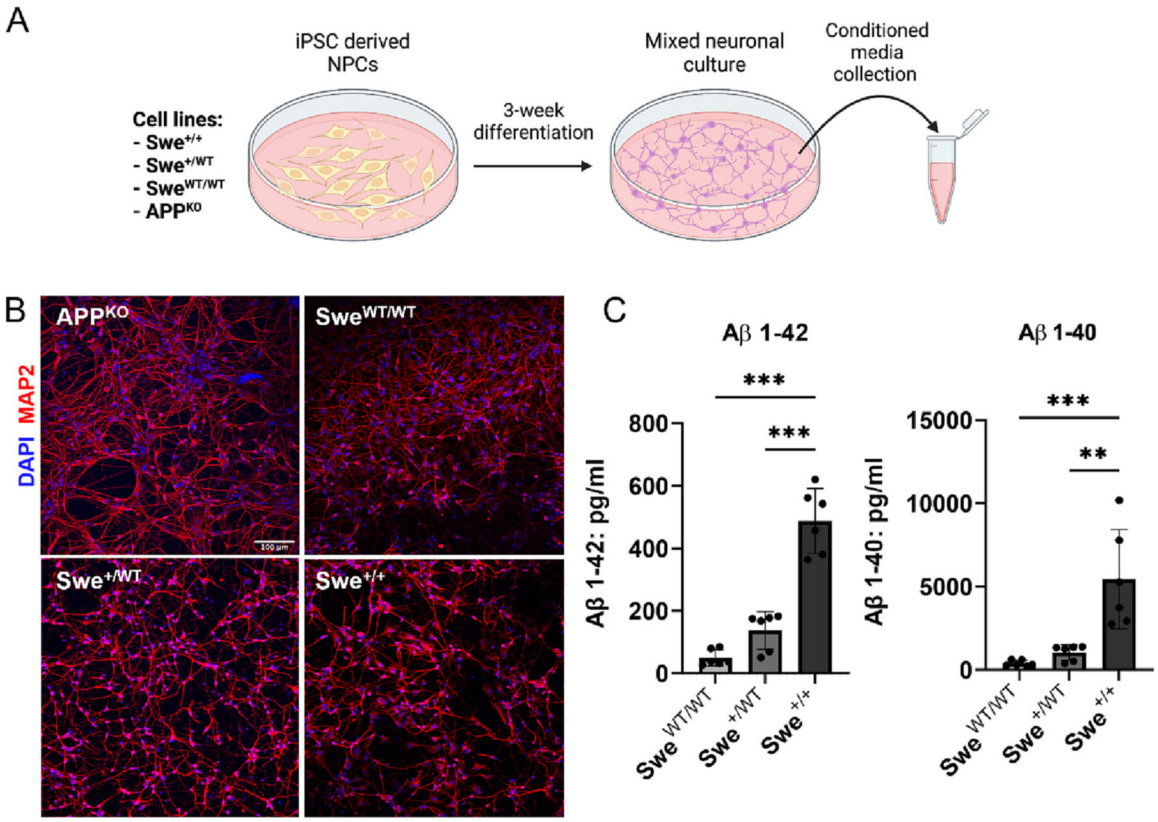

Fig. 1.

Condition media (CM) collection and characterization of hiPSC-CN cultures. (A) Schematic overview of CM obtained from neuronal cultures. $Swe^{+/+}$ (homozygous) and $Swe^{+/WT}$ (heterozygous) CNs were differentiated from hiPSCs harboring the APP Swedish mutation. For our controls, CNs were differentiated from an isogenic control line, $Swe^{WT/WT}$, and a line that has CRISPR knockout of the APP gene, APP^{KO}. (B) Immunofluorescent (IF) images of cortical neurons differentiated from APP^{KO}, $Swe^{WT/WT}$, $Swe^{+/WT}$, and $Swe^{+/+}$ hiPSCs show enriched staining for cortical neurons (MAP2, red). Scale bar: 100 μm (C) ELISA quantification of CM shows increased levels of Aβ expression in APPSwe CNs. $n = 3$ biological replicates. Error bars, mean ± SEM. $*p < 0.033$, $**p < 0.002$, and $***p < 0.001$ by one-way ANOVA with Tukey's correction for multiple comparisons test.

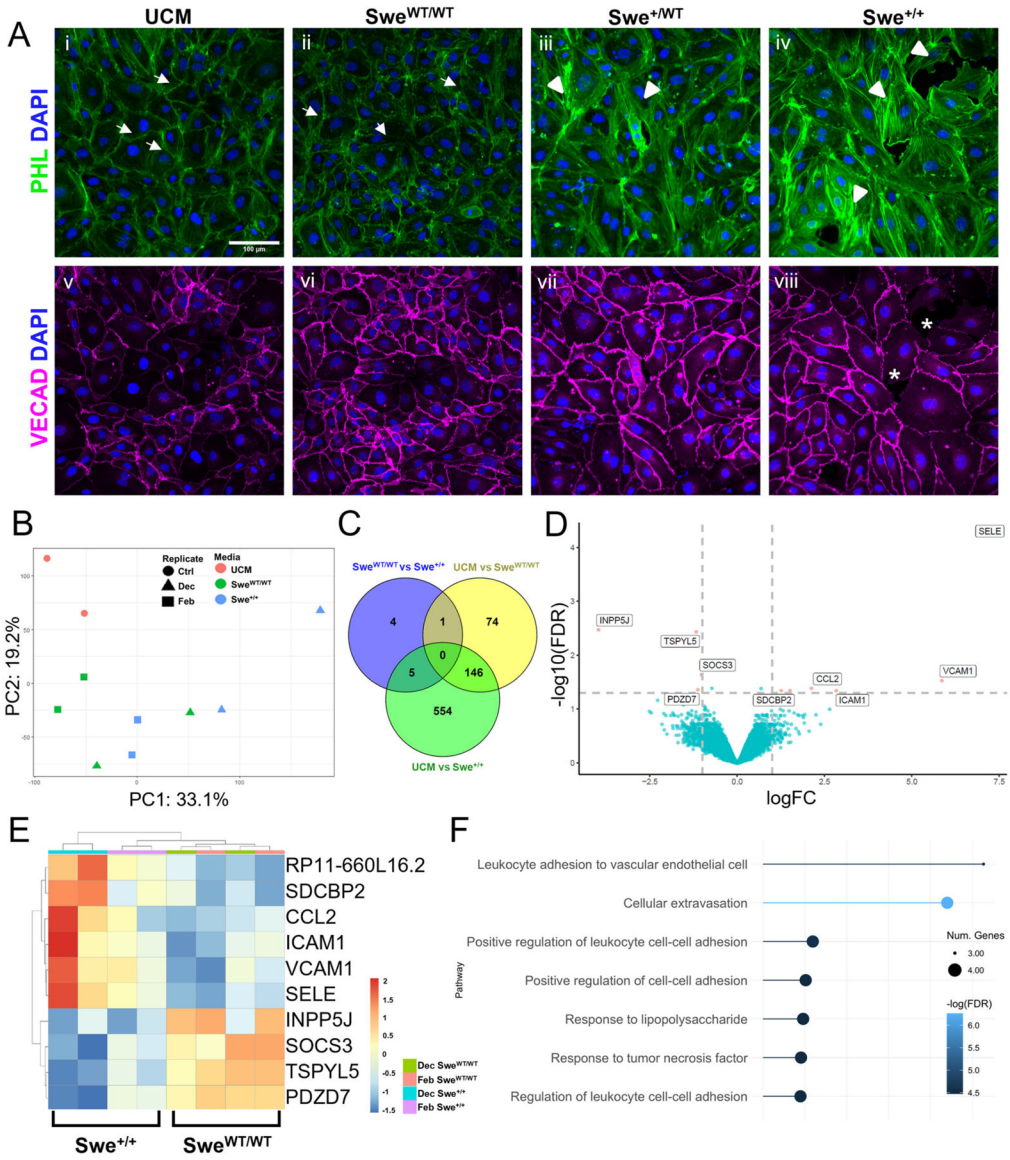

Fig. 2.

Cytoskeletal and transcriptomic changes in 2D HBMEC cultures after CM treatment. (A) Representative IF images of 2D cultured (i-viii) HBMECs treated with CM media. (ii) 2D cultures exposed to UCM and Swe$^{WT/WT}$ media maintain cortical actin cytoskeletal staining (Phalloidin, green) as denoted by white arrows (i and ii), Swe$^{+/WT}$ CM treatment shows endothelial retraction and f-actin stress fiber formation (Phalloidin, green) (iii) which is intensified in Swe$^{+/+}$ treatment (iv) as denoted by white arrow heads. Representative images from $n = 3$ biological replicates. 2D HBMEC IF staining shows good vascular endothelial cadherin junction (VECAD, magenta) in UCM, Swe$^{WT/WT}$, Swe$^{+/WT}$ CM treated HBMECs. (v-viii) Regional loss of VECAD is observed in Swe$^{+/+}$ CM treated HBMECs. (viii; asterisk) Scale bar: 100 μm (B) PCA of RNA-seq data from HBMECs treated with three media types (UCM, Swe$^{WT/WT}$ and Swe$^{+/+}$) in 2D. (C) Venn diagram showing the overlap of genes significantly changed by CM media treatment. 10 genes were

differentially expressed between $Swe^{WT/WT}$ and $Swe^{+/+}$ CM treatment. (D) Volcano plot showing DEGs between, $Swe^{WT/WT}$ treated media and $Swe^{+/+}$ treated media. (E) Heatmap of log counts per million (CPM) values for genes that were identified to be significant in $Swe^{+/+}$ treated HBMECs. (F) Gene Ontology terminology analysis for biological processes involved in upregulated genes in $Swe^{+/+}$ CM treated HBMECs.

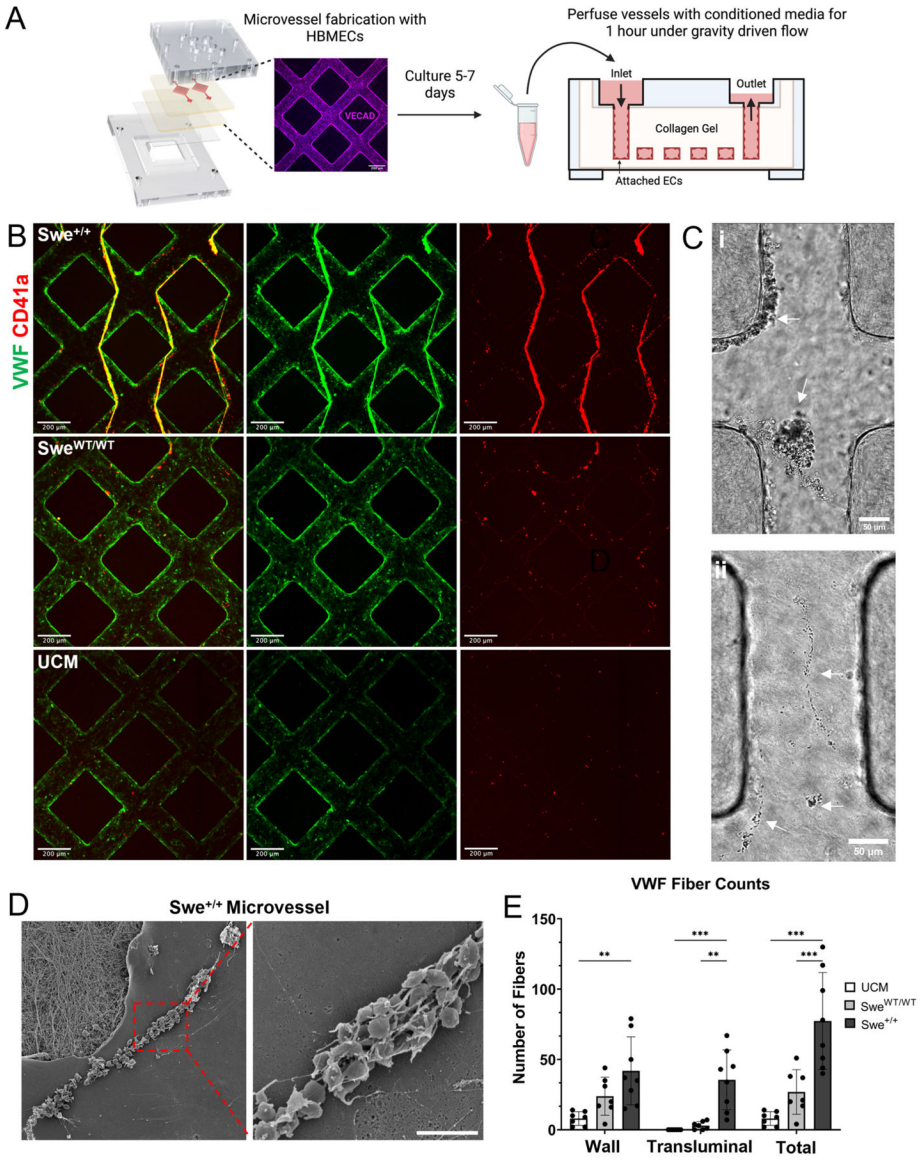

Fig. 3.

Perfusion of CM stimulates VWF release in 3D engineered cerebral microvessels.

(A) Schematic illustrating engineered microvessel fabrication and treatment of vessels with CM. (B) Representative images of microvessels treated with CM (bottom: unconditioned base media (UCM), middle: $Swe^{WT/WT}$, and top: $Swe^{+/+}$). $Swe^{+/+}$ CM perfusion causes VWF fiber formation (VWF, green) and induces binding of washed isolated platelets (CD41a, red). By comparison little to no VWF fiber formation or platelet binding occurs in UCM and $Swe^{WT/WT}$ CM treated microvessels. Scale bar: 200 μm. (C) Brightfield images of platelets binding to VWF fibers in engineered cerebral microvessels. Platelets bound to both (i) transluminal fibers and (ii) wall fibers. Arrows indicate platelet binding and aggregation. Scale bar: 50 μm. (D) SEM image of microvessels containing a wall VWF fiber with bound platelets. Platelets are bound in a mesh of VWF fibers present on the luminal surface of microvessels. Scale bar: 5 μm. (E) Quantification of VWF fibers formed upon perfusion of

engineered cerebral microvessels with CM. $n = 4$ biological replicates. Error bars, mean ± SEM. $*p < 0.05$, $**p < 0.01$, and $***p < 0.001$ by two-way ANOVA with Tukey's correction for multiple comparisons test.

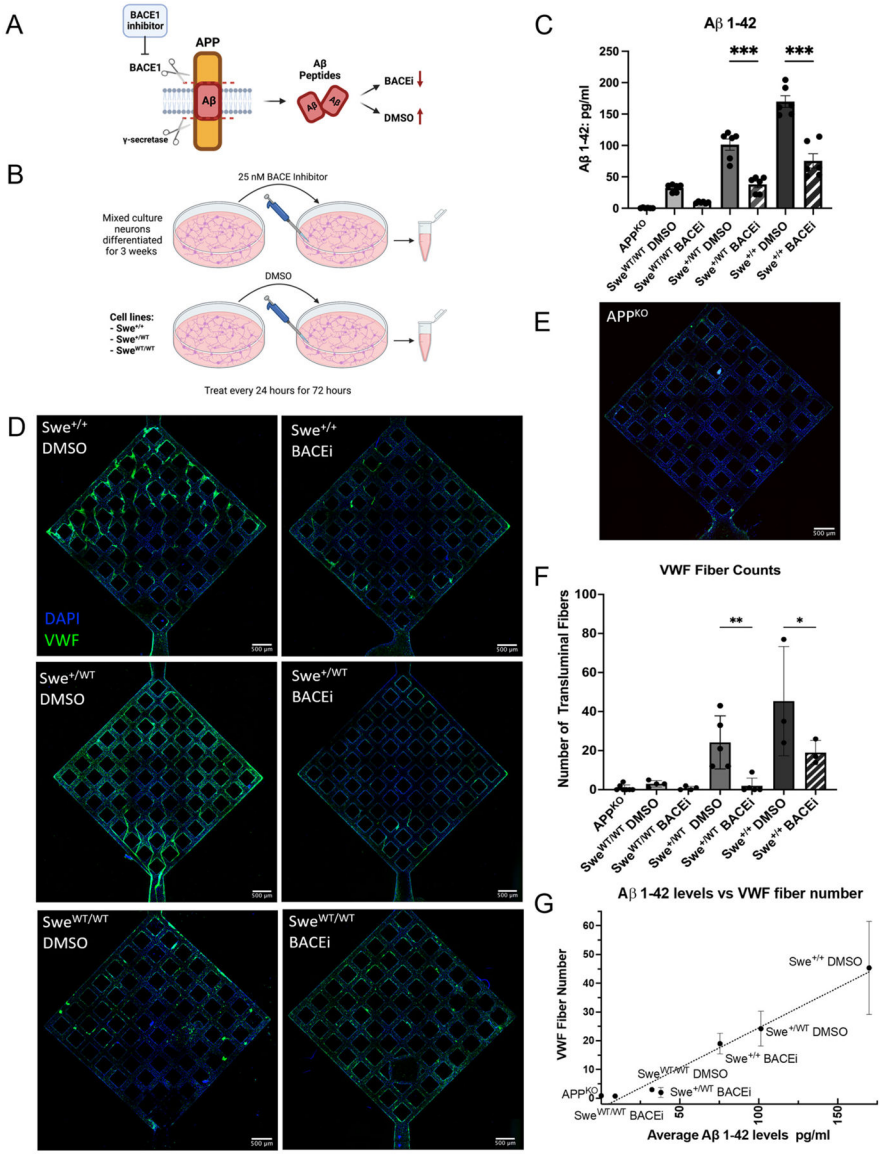

Fig. 4.

CM collected from BACE1 inhibitor (BACEi) treated neurons or APP^{KO} neurons cause reduced VWF fiber formation in 3D microvessels.

(A) BACEi mechanism of action. BACEi inhibits BACE1 cleavage of APP and results in decreased production amyloidogenic Aβ peptides. (B) Schematic overview showing CM collection from APPSwe neurons treated with BACEi or a DMSO vehicle control. BACEi CM and DMSO control CM were collected from CN differentiated from $Swe^{WT/WT}$, $Swe^{+/WT}$, and $Swe^{+/+}$ hiPSCs. (C) ELISA measurements confirm the reduction of pathogenic Aβ 1–42 production in BACEi and APP^{KO} conditions compared to the DMSO control. $n = 3$ biological replicates per condition. (D) Representative immunofluorescent images of 3D microvessels after perfusion with CM collected from $Swe^{WT/WT}$ neurons treated with DMSO (bottom left), $Swe^{WT/WT}$ neurons treated with BACEi (bottom right), $Swe^{+/WT}$ neurons treated with DMSO (middle left), $Swe^{+/WT}$ neurons treated with BACEi

(middle right), $Swe^{+/+}$ neurons treated with DMSO (top left), and $Swe^{+/+}$ neurons treated with BACEi (top right). BACEi CM results in a significant reduction in transluminal VWF fiber formation (VWF, green). Scale bars: 500 μm. (E) Representative IF image of 3D microvessels after perfusion with CM collected from APP^{KO} neurons. VWF transluminal fibers are absent from microvessels. Scale bars: 500 μm. (F) Quantification of transluminal fibers present in the microvessels. The number of transluminal fibers is significantly reduced in BACEi CM treated microvessels compared to the number of fibers formed in DMSO CM treated microvessels. $n = 4$ biological replicates. (G) Association between average Aβ 1–42 peptide levels and average VWF fiber number. Dotted black line is a linear least squares regression fit to the data points that shows a strong positive linear correlation (R-squared = 0.966, P value <0.001). All plots: error bars, mean ± SEM. *$p < 0.05$, **$p < 0.01$, and ***$p < 0.001$ by two-way ANOVA with Tukey's correction for multiple comparisons test (C), linear regression (G), or one-way ANOVA with Šídák's correction for multiple comparisons test.